Single-cycle SARS-CoV-2 vaccine elicits high protection and sterilizing immunity in hamsters

Thomas Klimkait (Thomas.Klimkait@unibas.ch)
University of Basel

Martin Lett
University of Basel

Fabian Otte
University of Basel https://orcid.org/0000-0003-0572-617X

David Hauser
University of Basel https://orcid.org/0000-0001-9950-365X

Jacob Schön
Friedrich Loeffler Institute https://orcid.org/0000-0002-9801-7972

Enja Kipfer
University of Basel

Donata Hoffmann
Friedrich Loeffler Institute https://orcid.org/0000-0003-4552-031X

Nico Halwe
Friedrich Loeffler Institut https://orcid.org/0000-0002-7983-2808

Angele Breithaupt
Friedrich-Loeffler-Institut https://orcid.org/0000-0002-6373-5923

Lorenz Ulrich
Institute of Diagnostic Virology, Friedrich-Loeffler-Institut, Federal Research Institute of animal health
https://orcid.org/0000-0001-5004-806X

Tobias Britzke
Friedrich-Loeffler-Institute

Yuepeng Zhang
University of Basel

Vladimir Cmiljanovic
RocketVax AG

Claudia Wylezich
Institute of Diagnostic Virology, Friedrich-Loeffler-Institut, Federal Research Institute of animal health
https://orcid.org/0000-0002-0436-4480

Lorena Urda
University of Basel

Christopher Lang

University of Basel

Martin Beer

Friedrich-Loeffler-Institute https://orcid.org/0000-0002-0598-5254

Christian Mittelholzer

University of Basel

Article

Keywords:

Posted Date: July 21st, 2023

DOI: https://doi.org/10.21203/rs.3.rs-3124718/v1

Additional Declarations: Yes there is potential Competing Interest. VC owns shares of RocketVax AG, Basel, CH. The other authors declare no competing interests. A patent application (no. WO 203/036947 A1) has been filed on the topic of this vaccine.

Single-cycle SARS-CoV-2 vaccine elicits high protection and sterilizing immunity in hamsters

Martin Joseph Lett[1,5], Fabian Otte[1,5], David Hauser[1,5], Jacob Schön[2], Enja Tatjana Kipfer[1], Donata Hoffmann[2], Nico J. Halwe[2], Angele Breithaupt[3], Lorenz Ulrich[2], Tobias Britzke[3], Yuepeng Zhang[1], Vladimir Cmiljanovic[4], Claudia Wylezich[2], Lorena Urda[1], Christopher Lang[1], Martin Beer[2], Christian Mittelholzer[4,6,7], Thomas Klimkait[1,6,8,*]

[1]Molecular Virology, Department of Biomedicine, University of Basel, 4009 Basel, Switzerland.
[2]Institute of Diagnostic Virology, Friedrich-Loeffler-Institute, Greifswald - Isle of Riems, Germany.
[3]Department of Experimental Animal Facilities and Biorisk Management, Friedrich-Loeffler-Institute, Greifswald - Isle of Riems, Germany.
[4]RocketVax AG, 4057 Basel, Switzerland.
[5,6]These authors contributed equally to this work.
[7]Current address: as [1]
[8]Lead contact
*Corresponding author: Thomas Klimkait (thomas.klimkait@unibas.ch)

Abstract

Vaccines have been central in ending the COVID-19 pandemic, but newly emerging SARS-CoV-2 variants increasingly escape first-generation vaccine protection. To fill this gap, live particle-based vaccines mimicking natural infection aim at protecting against a broader spectrum of virus variants. We designed “single-cycle SARS-CoV-2 viruses” (SCVs) that lack essential viral genes, possess superior immune-modulatory features and provide an excellent safety profile in the Syrian hamster model. All intranasally vaccinated animals were fully protected against an autologous challenge with SARS-CoV-2 virus using an Envelope-gene-deleted vaccine candidate. By deleting key immune-downregulating genes, sterilizing immunity was achieved with an advanced candidate without virus spread to contact animals. Furthermore, vaccinated animals were protected from SARS-CoV-2 characteristic tissue inflammation and lung damage. Hence, SCVs have the potential to induce broad and durable protection against COVID-19 superior to a natural infection.

Introduction

Since its first appearance in 2019, SARS-CoV-2 has spread rapidly worldwide and continues to circulate in many countries, causing symptoms and COVID-19 disease, despite an unprecedented, quick deployment of effective first-generation mRNA- and vector-based vaccines [1-5], targeting the viral Spike (S) protein. Since then, multiple virus variants have emerged, carrying escape mutations mainly in the S gene that correlate with declining protection rates [6,7].

To combat new variants of the virus and induce an immune response to additional viral proteins, recent vaccine approaches focus on attenuating the virus [8,9] and on intranasal applications for stronger induction of mucosal immunity [10]. One principal drawback of attenuated viral vaccines is the residual risk of an accidental reversion to virulence, i.e., causing the wild-type like disease from which one would like to protect [11,12]. This aspect is particularly crucial for key risk groups: immunocompromised, transplanted and elderly people, or cancer patients.

To generate a safe but effective SARS-CoV-2 vaccine with improved properties inducing a similarly broad immune response as live SARS-CoV-2 viruses, we designed a 'single-cycle infection concept'. The deletion of one essential structural gene from the viral genome, combined with a stable cellular trans-complementation system as used for other coronaviruses [13-16], leads to the production of intact but propagation-defective particles that may serve as SARS-CoV-2 vaccine candidates. We opted to eliminate the poorly immunogenic Envelope (E) gene and inserted an eGFP reporter in the reading frame of E (ΔE^G).

In addition, we deleted two of the accessory genes described to be crucial for down-modulating the anti-viral defense [17-19], creating a triple-deletion virus termed ΔE^G68 (Fig. 1a). Eliminating these SARS-CoV-2 accessory proteins, encoded e.g. by open reading frames (ORFs) ORF3a, ORF6, ORF7a, and ORF8 [20], is expected to increase the immunogenicity of

single-cycle viruses beyond that of a natural SARS-CoV-2 infection while retaining their safety, which is mainly based on the E gene deletion. In addition, ORF6 has been described to suppress T cell responses [17] and eliminate the interferon (IFN) response in the infected cell [18]. ORF8 had been shown to reduce the T-cell response *in vivo* [19].

This study thoroughly investigates the properties of a single-cycle, triple-deletion vaccine virus ($\Delta E^G 68$) and assesses the direct impact of eliminating ORF6 and ORF8 by comparing it to an "E-deleted only" vaccine virus (ΔE^G). We show evidence for enhanced immune stimulation, the elicitation of full protection against challenge infection, and for sterilizing immunity in the Syrian hamster model.

Results

Single-cycle virus stability and in vitro safety profile

Both SCV candidates were obtained using the ISA-based method described previously (Fig. 1a and Extended Data Fig. 1a, from design to vaccine virus in ~4 weeks) [21,22]. $\Delta E^G 68$ and ΔE^G were efficiently rescued in E-complementing HEK293T cells (HEK293T-indE) and propagated in a Vero E6-based cell line stably expressing the E protein (Vero-E2T). The presence and functionality of E in the established cell lines were assessed by mRNA detection (Extended Data Fig. 1b,c) or by virus complementation and propagation of cell-free progeny virus (Fig. 1b and Extended Data Fig. 1d-f). SCVs were monitored by antigen quick-tests [22] and quantified in focus formation assays (FFA).

The precise deletion of the three intended genes in vaccine virus candidate $\Delta E^G 68$ and of the E-gene in ΔE^G and their stable functional elimination were verified after repeated passage in Vero-E2T cells by NGS and Sanger sequencing. For candidate ΔE^G, a several log-fold increase of viral loads was observed upon repeated passaging, attributable to a spontaneous frame shift mutation in ORF3a that introduced a translational stop codon. Thus, for high multiplicity of infection (MOI) experiments and *in vitro* safety passaging, $\Delta E^G 3^*$ (ΔE^G with an

additional translational stop codon in ORF3a) was used. For animal safety data, the ΔE^G candidate was tested.

The single-cycle nature of the genetically modified vaccine candidates $\Delta E^G 68$ and ΔE^G was demonstrated by infecting standard Vero E6 cells that are commonly used for SARS-CoV-2 propagation: Even after a high MOI infection, detectable virus of either candidate quickly vanished from the culture supernatant, in contrast to *wild-type* infections during passaging (Fig. 1c). The possible emergence of viral revertants at sub-detection levels in Vero E6 cells was excluded by inoculating the producer cell line Vero-E2T for 6 days with supernatant samples from passages 1 to 10. As 1-5 focus-forming units (FFUs) are sufficient to initiate full viral amplification on Vero-E2T cells (Fig. 1b), an efficient propagation even of low-level revertants or newly emerging replicative viral variants would have been detected. None of the passages below 100 genomic copies/mL led to any rescuable replicative virus (Extended Data Fig. 1e,f).

In order to demonstrate that SCVs indeed represent authentic viral particles that package the defective genome, virions were analyzed by transmission electron microscopy, which confirmed the efficient production of spike-carrying spheres with the expected size of 80-100 nm typical for SARS-CoV-2 virions (Fig. 1d). To assess lower levels of viral S protein observed on the vaccine candidates, surface labeling of cells infected with SCVs or *wild-type* control was performed. Vaccine candidates show a strong S-signal at cell-to-cell interfaces compared to a more clustered staining of cells infected with *wild-type*. This indicates differences in viral assembly and particle formation (Extended Data Fig. 1g) [23].

Molecular characterization of vaccine candidates in vitro

We analyzed viral protein expression in infected Vero E6-TMPRSS2 cells (stable expression of TMPRSS2 in Vero E6 cells, Extended Data Fig. 1b) by immunoblotting and immunocytochemistry. As additional control we included the E-defective mutant E^{**fs} (two

back-to-back stop codons (*) and insertion of an additional G-nucleotide (frameshift (fs)) after the first 7 amino acids of E) that retains the RNA sequence and secondary structure to a large extent. At 24h post-infection, similar viral protein levels were found as for *wild-type* virus (Fig. 1e,f). The expression of NSP2 (non-structural protein 2, as reference for virus input), Nucleocapsid protein (N) and S was comparable, with elevated levels of cleaved S (subunit S1) only for the E^{**fs} mutant. For $\Delta E^{G}68$, absence of ORF6 and ORF8 was confirmed, while ORF7 as interjacent gene remained expressed in all tested variants. Immunoblot data also confirmed the expected ORF3a truncation in $\Delta E^{G}3^{*}$ due to the translational stop codon (Fig. 1e).

In summary, we observed for both $\Delta E^{G}68$ and ΔE^{G} vaccine candidates a close-to-*wild-type* expression level of all structural components, similar particle properties, and strict single-cycle infection in standard cells. This molecular characterization led us to verify the immunizing performance of our SC-vaccines *in vitro* and *in vivo*.

In vitro immuno-modulatory responses to vaccine candidates

Immune-downmodulating functions have been reported for ORF6 and ORF8 and to a lesser extent for the Envelope protein [17-19,24,25]. To test whether the lack of E, ORF6 and ORF8 in the SCV could provide a stronger immune response than *wild-type* virus, we transiently expressed each gene in monocytic THP-1 cells as a model for antigen-presenting cells (APCs). The impact of the newly introduced protein on immunological markers was then assessed by cell surface staining of antigen-presenting proteins (HLA-A/B/C, HLA-DR), the co-stimulators CD40, CD44, CD70, CD80 and CD275, and complement cascade protein (CD59). At 48 hours post-transfection, we observed a downregulation of CD80 and CD275 on THP-1 cells for all three proteins compared to a control plasmid (Fig. 2a-c), while no change was observed in the expression of HLA-DR and CD70, thus excluding labeling artefacts (Fig. 2a-c and Extended Data Fig. 2a). The direct effect on the HLA seems more modest (Extended Data Fig. 2b).

Taken together, these data indicate that the expression of ORF6, ORF8 and E correlates with a diminished presentation capacity on APCs. We then infected alveolar basal epithelial cells (A549) for 24 hours and stained them with the same panel, excluding HLA-DR. Two different SARS-CoV-2 strains served as controls: the original Wuhan strain (B.1), which is the basis of our mutants, and the recent Omicron XBB.1.5 strain, which naturally contains a premature stop codon at position 8 of ORF8, i.e., loss of ORF8 function as a result of natural selection (Extended Data Fig. 3a,b). A549 cells downregulated HLA-A/B/C and CD275 when infected with the Wuhan strain, but not with $\Delta E^{G}68$, whereas Omicron XBB.1.5 and E^{**fs} show only partial down-regulation, evoking a role of ORF8 (Fig. 2d,e). Similar effects are observed during the infection of HEK293T (Extended Data Fig. 2c-e).

Culture supernatants from infection of A549 or HEK293T cells were incubated with non-infectable THP-1 cells for 48 hours before staining (Extended Data Fig. 2f). Of interest, for HLA-A/B/C and CD80 we observed the same effect of the deletion as seen in overexpression experiments: while receptor expression was downregulated by *wild-type* infection, $\Delta E^{G}68$ SCV conversely induced a higher expression (Fig. 2f-i). The E^{**fs} mutant displayed intermediate expression levels, suggesting additive, non-overlapping functions of ORF6, ORF8 and E. The observation that the effect was seen on both infected and non-infectable cells suggests that these ORFs directly and indirectly impaired antigen presentation.

Vaccination and challenge infection in the Syrian hamster model

Our single-cycle vaccine concept was examined *in vivo* using the highest achievable dose for $\Delta E^{G}68$ or a low dose for the construct ΔE^{G}. Candidates or controls were administered intranasally to 5- to 6-week-old Syrian hamsters, an infection model used for safety and efficacy due to efficient viral spread [26]. Naïve contact hamsters were co-housed with immunized hamsters 24 hours after vaccine application, to be separated again for 24 hours only immediately before boost immunization or challenge infection (Fig. 3a).

159 Hamsters were immunized with $2.4*10^4$ FFUs of ΔE^G68 (n=12) or $3.5*10^2$ FFUs of ΔE^G (n=8)
160 in 100 μL per animal (Extended Data Fig. 4a,b). Following immunization, all animals
161 continually gained weight as expected (Fig. 3b,c). A minimal 'dip' in mean body weight on days
162 2-3 was observed in all experimental groups, including contact animals (Fig. 3b), and is typical
163 for and attributable to procedural stress. Since body weight loss usually occurs when Syrian
164 hamsters are inoculated with *wild-type* SARS-CoV-2, as shown by subsequent challenge
165 infection of sham-treated animals (Fig. 3d), this indicates that both vaccine candidates were
166 very well tolerated.
167 Already 19 days post immunization (dpim), profound SARS-CoV-2 specific humoral immune
168 responses were confirmed in all animals vaccinated with ΔE^G68 or ΔE^G and were even more
169 pronounced after the second immunization (33 dpim) (Fig. 3e).
170 The singe-cycle nature of ΔE^G68 and ΔE^G was confirmed by rapidly declining viral RNA signals
171 at 3 dpim ($10^{4,7}$ or $10^{3.8}$ mean genome copies/mL, resp.) and 7 dpim (10^2 or $10^{2.1}$ genome
172 copies/mL, resp.) after prime-immunization. This was close to or below the applied threshold
173 of the assay used (Fig. 3f, grey area).
174 On 3 dpim, two ΔE^G68 contacts became positive with a mean of $10^{3.5}$ genome copies/mL (Fig.
175 3f, light blue) as compared to the input of $2*10^6$ RNA copies administered per animal. An E-
176 gene-specific RT-qPCR assay [27] verified the deletion of E and excluded the possibility of a
177 reversion, which was further strengthened by the lack of clinical signs and the absence of any
178 further virus spread (Extended Data Table 2 and Fig. 3b-d,f). The low virus RT-qPCR signal
179 observed at 7 dpim for a single ΔE^G68 contact hamster was correlated with the presence of
180 SARS-CoV-2 specific antibodies on day 19 (Fig. 3e, light blue). However, based on the way
181 of sampling, we cannot exclude that during nasal washing, some tissue cells might have been
182 aspirated causing increased variance on 3 and 7 dpim.

After boost immunization, two out of 12 animals immunized with ΔE^G68 had an RNA signal on day 3. On day 7, no vaccine RNA remained detectable in any of the ΔE^G or ΔE^G68 immunized or contact animals (Fig. 3f).

Following homologous challenge with *wild-type* SARS-CoV-2 virus (~$10^{2.5}$ TCID, Wuhan B.1), no weight loss was observed in the ΔE^G68- and ΔE^G-vaccinated groups, while all sham-vaccinated animals lost body weight until 5 days post challenge infection (dpc) (Fig. 3d). Moreover, only very low viral loads, close to the threshold of quantification (grey area in Fig. 3g), were recovered from nasal washes on days 1, 2 and 4 after challenge infection of the ΔE^G68 vaccinated animals. This was in sharp contrast to and significantly different from the situation in sham-vaccinated animals ($p<0.0001$ for all three time points, Fig. 3g), in which 10^7-10^9 copies/mL were recovered. No viral genomes in nasal washing samples and no weight loss were observed in any of the 6 contact animals post challenge infection (Fig. 3g). This complete protection of the 6/6 contact animals strongly supports the notion of a sterilizing immunity achieved by the ΔE^G68 SC-vaccine.

Weight loss in ΔE^G contact animals was greatly delayed compared to infected controls starting only at day 3 (Fig. 3d). The difference in weight loss onset and severity can be explained by reduced virus shedding after challenge for ΔE^G immunized animals, which was significantly lower than in sham-immunized controls ($p<0.0001$ for 1, 2 and 4 dpc, Fig. 3g). At 4 dpc, the onset of prominent virus replication in the contact hamsters by far exceeded the shedding levels of the vaccinated animals (Fig. 3g).

It is interesting to note that the high levels of a pre-challenge antibody response did not further increase following challenge infection. This argues for a full response with maximal antibody induction already during the boost immunization phase, leading to a strong mucosal replication block of the challenge virus (Fig. 3h).

Upon detailed organ examination of ΔE^G68 immunized animals 5 dpc, a low viral load near the quantification limit was restricted to the nasal respiratory tract (grey area in Fig. 3i). On

day 14 post challenge, the RNA levels in the conchae of ΔE^{G}68-vaccinated animals were undetectable or below a quantifiable level. No signal was detected in the trachea or lungs of any of the animals (Fig. 3j).

For ΔE^{G}, RT-qPCR revealed quantifiable viral loads only in the conchae, calculated to be at least 50-fold lower than in the sham-immunized animals, and nearly complete protection from virus replication was confirmed in lung tissues (Fig. 3i). On day 14 dpc, the RT-qPCR signal in the conchae and the lower respiratory tract was greatly reduced. This indicates a high level of protection achieved with the SC vaccines.

Inflammation, tissue integrity and humoral immunity

A quantitative analysis of cytokine levels (IFNγ and IL-10) in homogenates of the conchae and the lungs 5 dpc showed up to 10-fold lower levels in ΔE^{G}68 vaccinated animals compared to sham animals (Fig. 4a,b). At 14 dpc, the comparison of vaccinated animals and their contacts suggests a lower interferon secretion for the ΔE^{G} vaccinated animals in both organs, but the low number of animals does not allow a precise comparison (Extended Data Fig. 4c). The absence of infection in contact animals of the ΔE^{G}68 group was corroborated by low cytokine secretion (Extended Data Fig. 4c,d).

Histopathology of the lung revealed full protection from infection-induced pulmonary atelectasis and SARS-CoV-2 characteristic lesions such as necrotizing bronchitis, vasculitis, and necrosis of the alveolar epithelium in ΔE^{G}68- and ΔE^{G}-vaccinated groups (Fig. 4c,d). However, minor findings were recorded in all groups (Extended Data Fig. 4e-h and Extended Data Table 3). Using immunohistochemistry, confluent to diffuse SARS-CoV-2 virus antigen was found in the lungs of sham-treated animals and was absent in ΔE^{G}68- and ΔE^{G}-vaccinated groups (Fig. 4d,f and Extended Data Table 3). At 14 dpc, ΔE^{G} contact animals showed minimal atelectasis and SARS-CoV-2 typical lesions, virus antigen was not

detectable. In clear contrast, no lesions were identified in lungs of ΔE^G68 contact animals (Fig. 4c-f, Extended Data Fig. 4e-h and Extended Data Table 3).

Neutralizing antibody responses were quantified against Wuhan (B.1). In 10 out of 12 ΔE^G68 vaccinated hamsters, neutralizing antibodies were already detectable after boost immunization (mean 1:229 for 100% neutralization dose) and remained stable after challenge for all vaccinated animals (5 dpc, 1:220; 14 dpc, 1:140) (Extended Data Table 4). For the ELISA-positive contact animal, a weak antibody response was detected on 33 dpim (1:40). For animals vaccinated with ΔE^G, neutralizing antibodies were detected after challenge infection (5 dpc, 1:404; 14 dpc, 1:295) (Extended Data Table 4). Notably, it can't be excluded that neutralization for ΔE^G would score positively before challenge, as the obtained serum volume was technically limiting to assess lower dilutions. Only one in four sham animals had a low titer (1:20), ruling out that the rise to neutralizing antibodies was based on the virus challenge. For all ΔE^G contact animals, a very low neutralization titer was apparent at 14 dpc (Extended Data Table 4).

Taken together, both vaccine candidates elicit high protection in the Syrian hamster. In addition, the deletion of ORF6 and ORF8 led to a sterilizing immunity in all vaccinated animals potentially due to a stronger immune response by IFN-mediated signaling, improved immune stimulation and/or higher vaccine inoculum.

Discussion

Efficient vaccines must have key properties to generate an immune response. First, providing or generating enough targets recognized by host antibodies, and second, inducing sufficient activation of T lymphocytes. In addition to strong immunogenicity, it is essential to ensure maximum safety. The two vaccine candidates reported here combine these properties. Our single-cycle vaccine generates *wild-type* like viral particles, which induce an accumulation of viral proteins in the host cell, serving as targets for B and T cells. This implies that efficient

260 replication of viral RNA has occurred. Deletion of ORF6 and ORF8, two anti-inflammatory
261 proteins that antagonize T cell activation, further supports a strong host response as
262 suggested by our *in vitro* data and published literature [17-19,23,24].
263 We show that our candidate ΔE^{G}68 causes higher surface expression of HLA molecules and
264 co-stimulatory factors on infected cells or surrounding APCs, in particular CD80 (B7-1) and
265 CD275 (B7-H1/ICOSLG), both involved in T cell stimulation [28,29]. Notably, humans with a
266 defective CD275 gene produce low levels of IgG, IgA, and memory B cells [30]. The measurable
267 effect on infected cells, but also on non-infectable cells in contact, suggests an indirect effect
268 through local inflammation. These elements argue for greater immunogenicity of the SCV
269 compared to its native counterpart.
270 Maximum safety of our vaccine approach is ensured by the demonstrated single-cycle
271 concept. This prevents viral propagation, and unlike an attenuated virus approach, which
272 relies on the immune system to combat a weakened virus, could enable the use in
273 immunocompromised people.
274 Furthermore, we achieved sterilizing immunity for ΔE^{G}68 in Syrian hamsters, a characteristic
275 that is fundamental to preventing viral spread in humans and that has not been achieved in
276 other vaccine candidates so far [31,32]. This might be due to enhanced local immunity after nasal
277 application, which prevents viral shedding [33], demonstrated by a more profound immune
278 response with ΔE^{G}68 virus compared to *wild-type* infection.
279 The analysis of cytokine secretion additionally highlights the remarkable efficiency of the SCV
280 concept. In the conchae and in the lungs less signs of local inflammation were seen at 5 dpc
281 in the ΔE^{G}68 vaccinated animals, supporting the hypothesis of an infection that has already
282 resolved, also indicated by the absence of viral antigens. This is further supported by the
283 absence of pulmonary lesions observed in histological sections.
284 Interestingly, we observed transmission of high dose ΔE^{G}68 vaccine to one of six contact
285 animals. Spontaneous genetic reversion was excluded by RT-qPCR. No further propagation

or weight loss was observed, indicating a passive transfer of the vaccine virus. The transfer was accompanied by seroconversion, implying that even a very small dose of SCV is sufficient to induce a high serological response.

It should be mentioned here that we had to repeat one SARS-CoV-2 challenge infection due to an erroneous over-dilution with no detection of infectious challenge virus (see Materials and Methods). However, all experimental data confirm that this had no influence on the overall results and that the repeated challenge infection could be classified as valid.

Taken together, our proposed single-cycle vaccine concept consolidates the high safety of an intranasally applied vaccine that induces sterilizing immunity, which will be key to overcoming the ongoing SARS-CoV-2 outbreaks.

References

1 Beesley, L. J. *et al.* SARS-CoV-2 variant transition dynamics are associated with vaccination rates, number of co-circulating variants, and convalescent immunity. *EBioMedicine* **91**, 104534 (2023). https://doi.org:10.1016/j.ebiom.2023.104534

2 Baden, L. R. *et al.* Efficacy and Safety of the mRNA-1273 SARS-CoV-2 Vaccine. *N Engl J Med* **384**, 403-416 (2021). https://doi.org:10.1056/NEJMoa2035389

3 Polack, F. P. *et al.* Safety and Efficacy of the BNT162b2 mRNA Covid-19 Vaccine. *N Engl J Med* **383**, 2603-2615 (2020). https://doi.org:10.1056/NEJMoa2034577

4 Sadoff, J. *et al.* Final Analysis of Efficacy and Safety of Single-Dose Ad26.COV2.S. *N Engl J Med* **386**, 847-860 (2022). https://doi.org:10.1056/NEJMoa2117608

5 Voysey, M. *et al.* Safety and efficacy of the ChAdOx1 nCoV-19 vaccine (AZD1222) against SARS-CoV-2: an interim analysis of four randomised controlled trials in Brazil, South Africa, and the UK. *Lancet* **397**, 99-111 (2021). https://doi.org:10.1016/S0140-6736(20)32661-1

6 Tseng, H. F. *et al.* Effectiveness of mRNA-1273 against SARS-CoV-2 Omicron and Delta variants. *Nat Med* **28**, 1063-1071 (2022). https://doi.org:10.1038/s41591-022-01753-y

7 Muik, A. *et al.* Neutralization of SARS-CoV-2 Omicron by BNT162b2 mRNA vaccine–elicited human sera. *Science* **375**, 678-680 (2022). https://doi.org:10.1126/science.abn7591

8 Wang, Y. *et al.* Scalable live-attenuated SARS-CoV-2 vaccine candidate demonstrates preclinical safety and efficacy. *Proc Natl Acad Sci U S A* **118** (2021). https://doi.org:10.1073/pnas.2102775118

9 Nouailles, G. *et al.* Live-attenuated vaccine sCPD9 elicits superior mucosal and systemic immunity to SARS-CoV-2 variants in hamsters. *Nat Microbiol* (2023). https://doi.org:10.1038/s41564-023-01352-8

10 Afkhami, S. *et al.* Respiratory mucosal delivery of next-generation COVID-19 vaccine provides robust protection against both ancestral and variant strains of SARS-CoV-2. *Cell* **185**, 896-915 e819 (2022). https://doi.org:10.1016/j.cell.2022.02.005

11 Minor, P. D. The molecular biology of poliovaccines. *J Gen Virol* **73 (Pt 12)**, 3065-3077 (1992). https://doi.org:10.1099/0022-1317-73-12-3065

12 Platt, L. R., Estivariz, C. F. & Sutter, R. W. Vaccine-associated paralytic poliomyelitis: a review of the epidemiology and estimation of the global burden. *J Infect Dis* **210 Suppl 1**, S380-389 (2014). https://doi.org:10.1093/infdis/jiu184

13 Almazan, F. *et al.* Engineering a replication-competent, propagation-defective Middle East respiratory syndrome coronavirus as a vaccine candidate. *mBio* **4**, e00650-00613 (2013). https://doi.org:10.1128/mBio.00650-13

14 Gutierrez-Alvarez, J. *et al.* Middle East respiratory syndrome coronavirus vaccine based on a propagation-defective RNA replicon elicited sterilizing immunity in mice. *Proc Natl Acad Sci U S A* **118** (2021). https://doi.org:10.1073/pnas.2111075118

15 Zhang, X. *et al.* A trans-complementation system for SARS-CoV-2 recapitulates authentic viral replication without virulence. *Cell* **184**, 2229-2238.e2213 (2021). https://doi.org:10.1016/j.cell.2021.02.044

16 Netland, J. *et al.* Immunization with an attenuated severe acute respiratory syndrome coronavirus deleted in E protein protects against lethal respiratory disease. *Virology* **399**, 120-128 (2010). https://doi.org:10.1016/j.virol.2010.01.004

17 Yoo, J. S. *et al.* SARS-CoV-2 inhibits induction of the MHC class I pathway by targeting the STAT1-IRF1-NLRC5 axis. *Nat Commun* **12**, 6602 (2021). https://doi.org:10.1038/s41467-021-26910-8

18 Kimura, I. *et al.* Sarbecovirus ORF6 proteins hamper induction of interferon signaling. *Cell Rep* **34**, 108916 (2021). https://doi.org:10.1016/j.celrep.2021.108916

19 Zhang, Y. *et al.* The ORF8 protein of SARS-CoV-2 mediates immune evasion through down-regulating MHC-Iota. *Proc Natl Acad Sci U S A* **118** (2021). https://doi.org:10.1073/pnas.2024202118

20 Silvas, J. A. *et al.* Contribution of SARS-CoV-2 Accessory Proteins to Viral Pathogenicity in K18 Human ACE2 Transgenic Mice. *J Virol* **95**, e0040221 (2021). https://doi.org:10.1128/JVI.00402-21

21 Melade, J. *et al.* A simple reverse genetics method to generate recombinant coronaviruses. *EMBO Rep* **23**, e53820 (2022). https://doi.org:10.15252/embr.202153820

22 Kipfer, E. T. *et al.* Rapid cloning-free mutagenesis of new SARS-CoV-2 variants using a novel reverse genetics platform. *bioRxiv*, 2023.2005.2011.540343 (2023). https://doi.org:10.1101/2023.05.11.540343

23 Cattin-Ortola, J. *et al.* Sequences in the cytoplasmic tail of SARS-CoV-2 Spike facilitate expression at the cell surface and syncytia formation. *Nat Commun* **12**, 5333 (2021). https://doi.org:10.1038/s41467-021-25589-1

24 Chen, I. P. *et al.* Viral E protein neutralizes BET protein-mediated post-entry antagonism of SARS-CoV-2. *Cell Rep* **40**, 111088 (2022). https://doi.org:10.1016/j.celrep.2022.111088

25 Vann, K. R. *et al.* Binding of the SARS-CoV-2 envelope E protein to human BRD4 is essential for infection. *Structure* **30**, 1224-1232 e1225 (2022). https://doi.org:10.1016/j.str.2022.05.020

26 Sia, S. F. *et al.* Pathogenesis and transmission of SARS-CoV-2 in golden hamsters. *Nature* **583**, 834-838 (2020). https://doi.org:10.1038/s41586-020-2342-5

27 Corman, V. M. *et al.* Detection of 2019 novel coronavirus (2019-nCoV) by real-time RT-PCR. *Euro Surveill* **25** (2020). https://doi.org:10.2807/1560-7917.ES.2020.25.3.2000045

28 Yu, X., Fournier, S., Allison, J. P., Sharpe, A. H. & Hodes, R. J. The role of B7 costimulation in CD4/CD8 T cell homeostasis. *J Immunol* **164**, 3543-3553 (2000). https://doi.org:10.4049/jimmunol.164.7.3543

29 Wong, S. C., Oh, E., Ng, C. H. & Lam, K. P. Impaired germinal center formation and recall T-cell-dependent immune responses in mice lacking the costimulatory ligand B7-H2. *Blood* **102**, 1381-1388 (2003). https://doi.org:10.1182/blood-2002-08-2416

30 Roussel, L. & Vinh, D. C. ICOSL in host defense at epithelial barriers: lessons from ICOSLG deficiency. *Curr Opin Immunol* **72**, 21-26 (2021). https://doi.org:10.1016/j.coi.2021.03.001

31 Jung, J. *et al.* Transmission and Infectious SARS-CoV-2 Shedding Kinetics in Vaccinated and Unvaccinated Individuals. *JAMA Netw Open* **5**, e2213606 (2022). https://doi.org:10.1001/jamanetworkopen.2022.13606

32 Martinez-Baz, I. *et al.* Effect of COVID-19 vaccination on the SARS-CoV-2 transmission among social and household close contacts: A cohort study. *J Infect Public Health* **16**, 410-417 (2023). https://doi.org:10.1016/j.jiph.2023.01.017

33 Miteva, D. *et al.* Mucosal COVID-19 vaccines: Risks, benefits and control of the pandemic. *World J Virol* **11**, 221-236 (2022). https://doi.org:10.5501/wjv.v11.i5.221

34 Thi Nhu Thao, T. *et al.* Rapid reconstruction of SARS-CoV-2 using a synthetic genomics platform. *Nature* **582**, 561-565 (2020). https://doi.org:10.1038/s41586-020-2294-9

35 Chu, D. K. W. *et al.* Molecular Diagnosis of a Novel Coronavirus (2019-nCoV) Causing an Outbreak of Pneumonia. *Clin Chem* **66**, 549-555 (2020). https://doi.org:10.1093/clinchem/hvaa029

36 Protocol: Real-time RT-PCR assays for the detection of SARS-CoV-2 Institut Pasteur, Paris.

37 Wernike, K. *et al.* Multi-species ELISA for the detection of antibodies against SARS-CoV-2 in animals. *Transbound Emerg Dis* **68**, 1779-1785 (2021). https://doi.org:10.1111/tbed.13926

38 Stegmann, K. M. *et al.* Inhibitors of dihydroorotate dehydrogenase cooperate with molnupiravir and N4-hydroxycytidine to suppress SARS-CoV-2 replication. *iScience* **25**, 104293 (2022). https://doi.org:https://doi.org/10.1016/j.isci.2022.104293

39 Breithaupt, A., Sick, F., Golender, N., Beer, M. & Wernike, K. Characterization of experimental Shuni virus infection in the mouse. *Veterinary Pathology* **60**, 341-351 (2023). https://doi.org:10.1177/03009858231155402

40 Bussmann, B. M., Reiche, S., Jacob, L. H., Braun, J. M. & Jassoy, C. Antigenic and cellular localisation analysis of the severe acute respiratory syndrome coronavirus nucleocapsid protein using monoclonal antibodies. *Virus Res* **122**, 119-126 (2006). https://doi.org:10.1016/j.virusres.2006.07.005

41 Rihn, S. J. *et al.* A plasmid DNA-launched SARS-CoV-2 reverse genetics system and coronavirus toolkit for COVID-19 research. *PLoS Biol* **19**, e3001091 (2021). https://doi.org:10.1371/journal.pbio.3001091

42 Miyamoto, Y. *et al.* SARS-CoV-2 ORF6 disrupts nucleocytoplasmic trafficking to advance viral replication. *Commun Biol* **5**, 483 (2022). https://doi.org:10.1038/s42003-022-03427-4

Fig. 1: Single-cycle vaccine concept and viral characterization

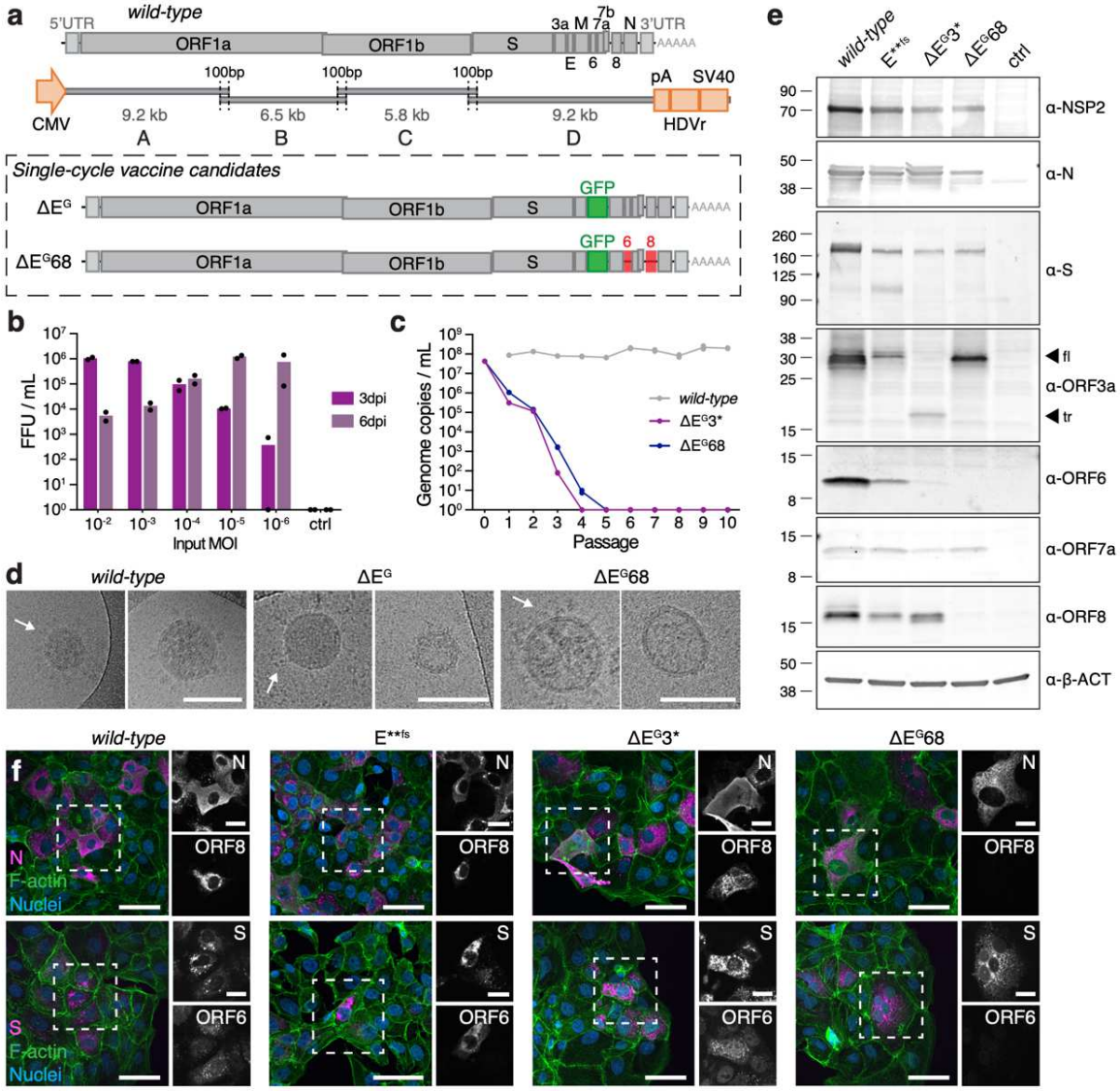

418

Fig. 1: Single-cycle vaccine concept and viral characterization

a, Schematic illustrating the SARS-COV-2 genomic landscape and the deletions/substitutions in ΔE^{G}/ΔE^{G}68, main structural and accessory proteins indicated. Four overlapping fragments covering the whole SARS-CoV-2 genome were amplified by PCR (Fragments A-D, see also Extended Data Figure 1a).

b, Complementation efficiency of Vero-E2T cells, analyzed by FFA (focus forming assay) of ΔE^{G}3* infection at different MOI or medium-only control (ctrl) after 3 and 6 dpi (n=2 individual cultures), for corresponding genome copies, see Extended Data Fig. 1d.

c, Passaging of 1:10 and 1:100 (after p2) dilutions of cell-free supernatant (Input = Passage 0) of wild-type SARS-CoV-2 (Muc-1, B.1), ΔE^{G}3* and ΔE^{G}68 on non-complementing Vero E6 cells (initial infection MOI = 1). Data from one representative experiment are shown; analysis was performed in duplicates.

d, Transmission electron microscopy analysis of recombinant wild-type SARS-CoV-2 (rCoV2) or vaccine candidates ΔE^{G} and ΔE^{G}68 showing the presence of the characteristic spike protein (indicated with arrows).

e, Immunoblot analysis of viral protein production in Vero E6-TMPRSS2 cells infected with rCoV2, E**fs, ΔE^{G}3*, ΔE^{G}68 or medium only (ctrl), probed with anti-NSP2, anti-N, anti-S, anti-ORF3a (full-length (fl) and truncated (tr) forms indicated with arrows), anti-ORF6, anti-ORF7a, anti-ORF8, and anti-beta-actin (β-ACT) antibodies.

f, Detection of N and S (magenta), F-actin (green), nuclei (blue) and ORF6 or ORF8 in Vero E6-TMPRSS2 cells infected with rCoV2, E**fs, ΔE^{G}3* or ΔE^{G}68.

Scale bar is 100nm in (**f**), 50μm and 20μm in (**e**) and (**f**) (overview and ROI images, respectively).

Fig. 2: Immunomodulation by E, ORF6 and ORF8 proteins

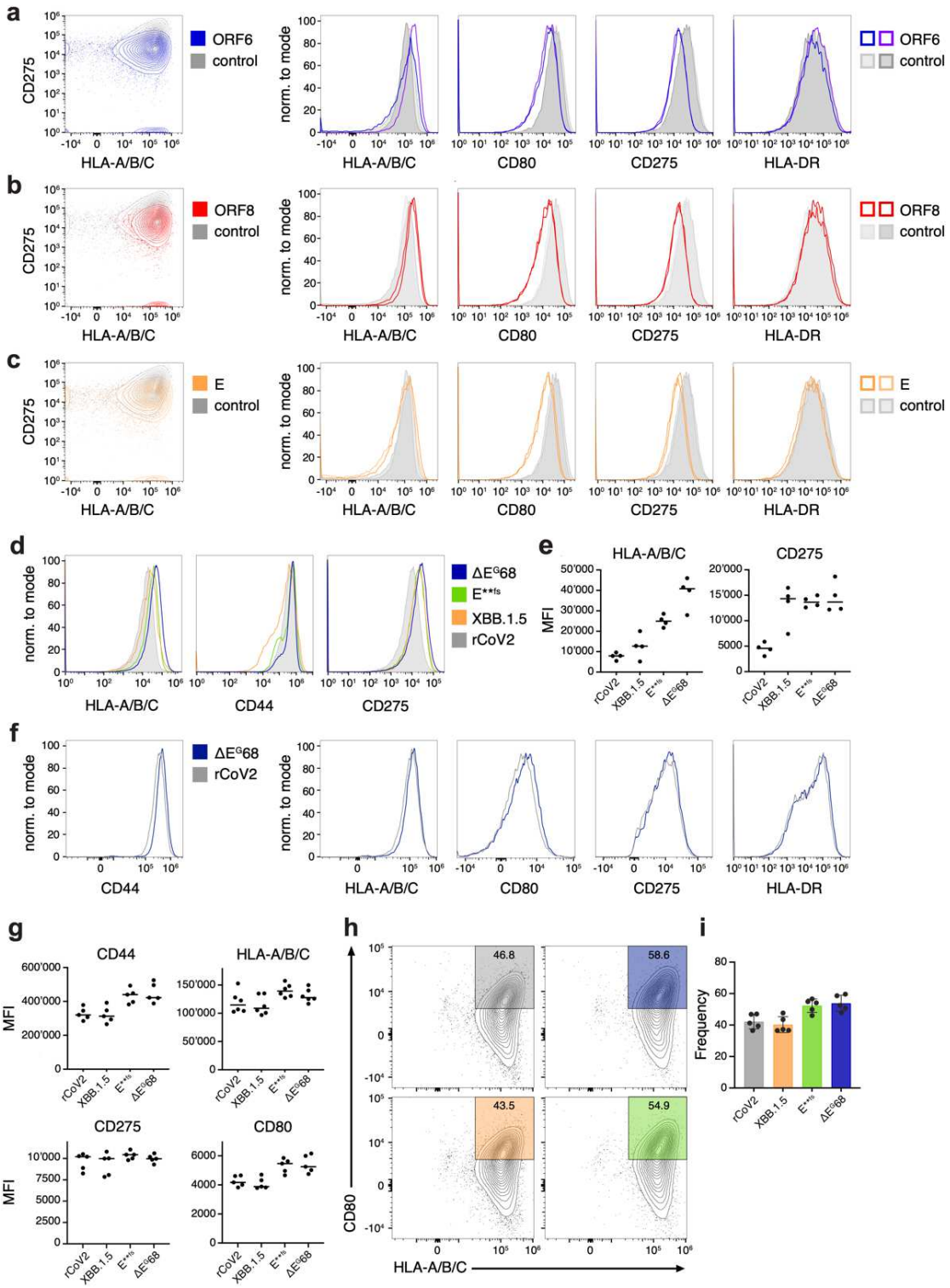

442

Fig. 2: Immunomodulation by E, ORF6 and ORF8 proteins

a-c, Modulation after transfection: Flow cytometry staining of THP-1 cells for HLA-A/B/C, CD80, CD275, and HLA-DR surface expression 48h after transfection with expression plasmids for ORF6 (**a**), ORF8 (**b**), or Envelope (**c**) proteins, compared with control transfection.

d-i, Modulation after infection: A549-ACE2-TMPRSS2 cells were infected with rCoV2, E**fs, $\Delta E^{G}68$, or XBB.1.5 SARS-CoV-2 virus (MOI = 0.1) for 24h, and stained for HLA-A/B/C, CD44 and CD275. **e,** Median fluorescence intensity (MFI) of HLA-A/B/C and CD274. The same infection was conducted on HEK293T and their respective supernatant is then applied on THP-1 for 48h before surface staining and analysis. **f,** Histogram showing the expression of CD44, HLA-A/B/C, CD80, CD275, and HLA-DR on THP-1 after 48 h. **g,** Median fluorescence intensity of HLA-A/B/C, CD80, and CD275 marker on THP-1 after 48 h incubation. The downregulation of the HLA and co-molecule can be seen when full-length virus is used as seen in the dot plot (**h**) comparing wild-type or $\Delta E^{G}68$ condition for their expression of CD80 and HLA-A/B/C. The frequency of cells outside of the gate in (**h**) is shown in (**i**).

Fig. 3: Immunization and challenge infection of Syrian hamsters

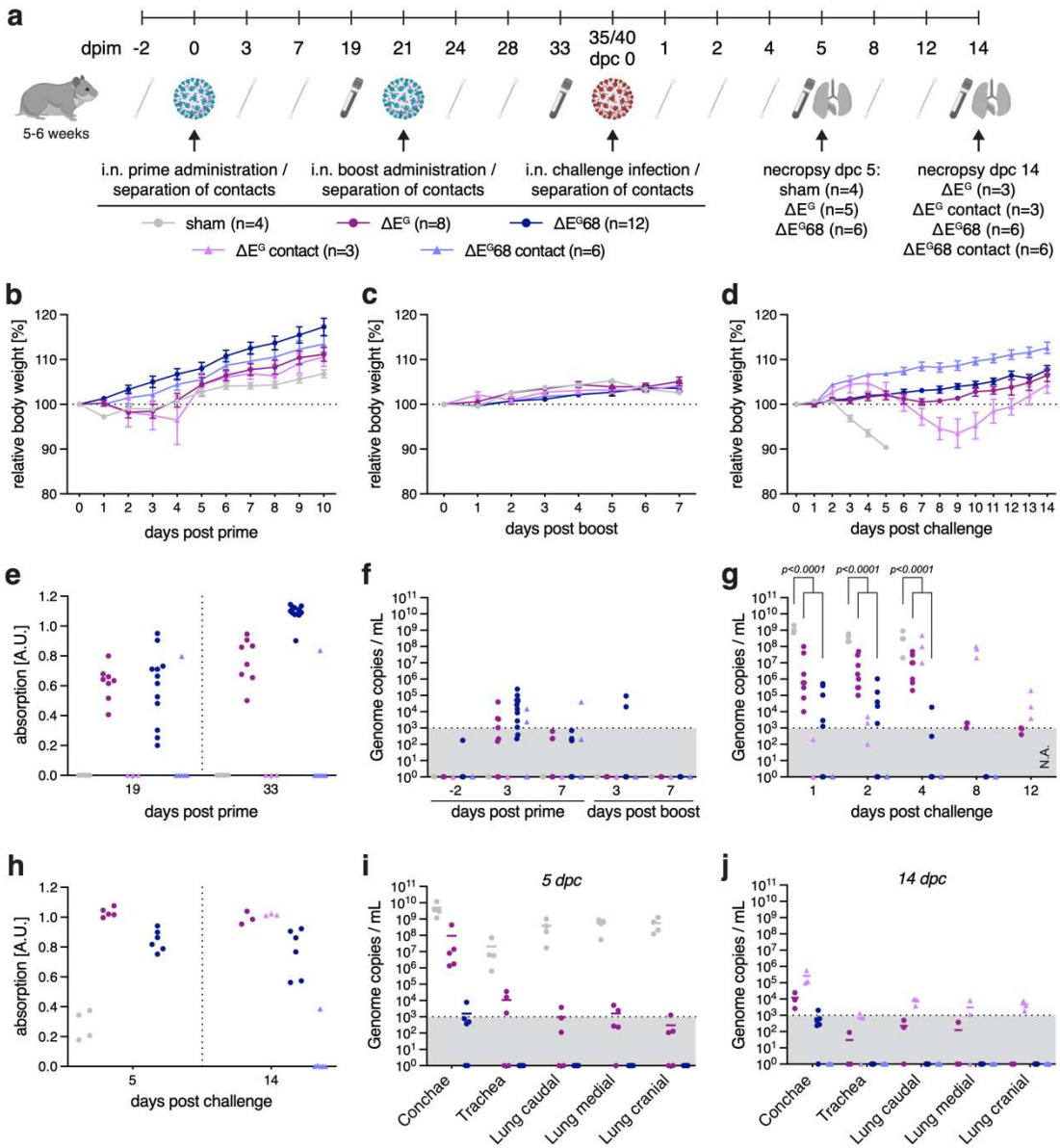

458

Fig. 3: Immunization and challenge infection of Syrian hamsters

a, Experimental setup and timeline including a prime-boost-immunization and subsequent virus challenge. At indicated time points serum and nasal washing samples were taken. Organ samples were obtained on the days of necropsy. Serum samples were used to detect SARS-CoV-2 RBD (receptor binding domain)-specific antibodies by ELISA or neutralizing antibodies. Genomic RNA loads in nasal washings and organ samples were investigated by SARS-CoV-2 polymerase gene-specific RT-qPCR.

b-d, Relative body weight after intranasal prime (**b**), boost immunization (**c**) and challenge infection (**d**).

e, Humoral immune response after prime and boost immunization (dpim 19 and 33, resp.), determined by ELISA against the SARS-CoV-2 RBD of S.

f,g, Virus genome copy numbers detected in nasal washing samples following prime and boost immunization (**f**) and challenge infection (**g**) (note: no data available for $\Delta E^{G}68$ and $\Delta E^{G}68$ contact animals at 12 dpc in (**g**)).

h, Humoral immune response after challenge (5 and 14 dpc), determined by SARS-CoV-2 RBD specific ELISA.

i,j, Viral genome copies in organ samples 5 dpc (**i**) and 14 dpc (**j**).

Mean and S.E.M. (**b**, **c** and **d**), scatter plots (**i** and **j**) show mean values as line, two-way anova followed by Bonferroni's test (**g**).

Fig. 4: Inflammation and tissue integrity

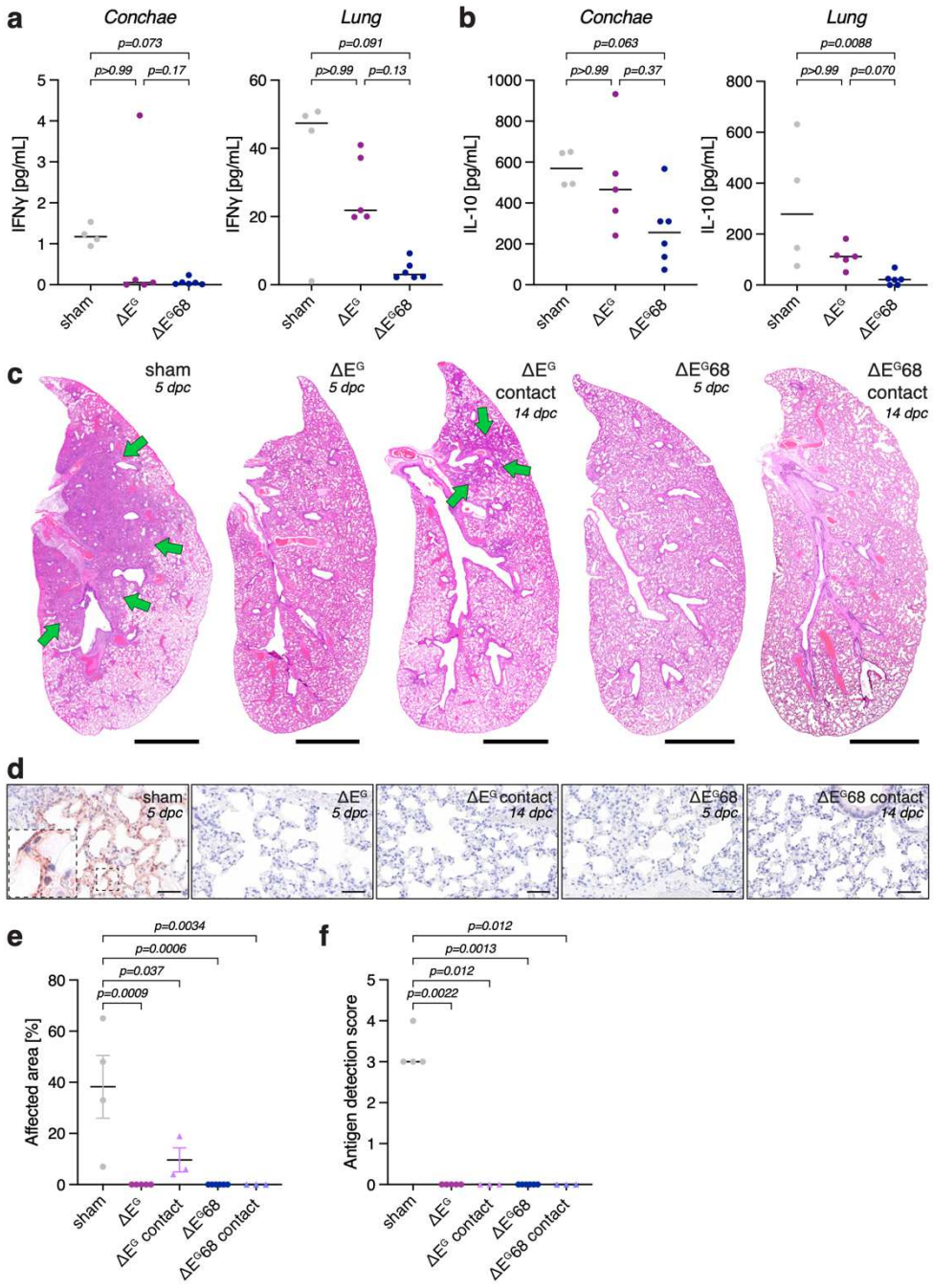

478

Fig. 4: Inflammation and tissue integrity

a,b, Cytokine levels in conchae and lungs of ΔE^G68, ΔE^G and sham-vaccinated hamsters 5 dpc, ELISA for IFNγ (**a**) and IL-10 (**b**).

c,e, Lung histopathology in ΔE^G68, ΔE^G and sham-vaccinated hamsters or contact animals, 5 or 14 dpc, respectively. **c,** Representative whole-slide images of lungs (affected area indicated with green arrows) and quantification (**e**) of infection-induced pulmonary atelectasis, affected area per lung lobe. Hematoxylin-Eosin stain, one slide per animal, blind to treatment.

d,f, Virus antigen detection in lungs of ΔE^G68, ΔE^G and sham-vaccinated hamsters or contact animal, 5 or 14 dpc, respectively. **d,** Representative immunohistochemistry images showing SARS-CoV-2 nucleocapsid protein detection and quantification (**f**) with virus antigen score (semiquantitative, 0 = no antigen, 1 = focal, 2 = multifocal, 3 = coalescing, 4 = diffuse) (Extended Data Table 3). One slide per animal, blind to treatment.

Number of animals: ΔE^G68 (n=6), ΔE^G (n=5), sham-vaccinated hamsters (n=4), contact animals (n=3 for both groups)

Median (**a**, **b** and **f**) or mean and S.E.M. (**e**), Kruskal-Wallis (**a**, **b**, **f**) or one-way anova (**e**) followed by Dunn's or Bonferroni's multiple comparisons test, respectively.

Scale bar is 2.5mm in (**c**) and 100 μm in (**d**).

Methods

Animals

All procedures involving animals were evaluated by the responsible ethics committee of the State Office of Agriculture, Food Safety, and Fishery in Mecklenburg–Western Pomerania (LALLF M-V) and gained governmental approval under the registration numbers LVL MV TSD/ 7221.3-1-041/20. Specific pathogen-free male Syrian hamsters (*Mesocricetus auratus*) (Janvier labs, RjHan:AURA) were kept at 20 to 22°C and a relative humidity of 45 ± 10% on a 12-hour light/dark cycle, fed with commercial rodent chow (Ssniff, Soest, Germany), and provided with water ad libitum. Age of the animals at prime immunization is 5 weeks for ΔE^{G} and 6 weeks for $\Delta E^{G}68$. Generally, hamsters underwent a daily physical examination and bodyweight routine.

Cell lines

African green monkey kidney cells (Vero E6) were kindly provided by V. Thiel, Bern, Switzerland, or obtained from the Collection of Cell Lines in Veterinary Medicine CCLV-RIE 0929. Adenocarcinomic human alveolar basal epithelial cells (A549) were obtained from NIBSC (A549-ACE-2 Clone 8-TMPRSS2; product number 101006). The THP-1 myelomonocytic leukemia cell line was obtained from the American Type Culture Collection. HEK293T cells were kindly provided by D. D. Pinschewer. For the generation of HEK293T-E, HEK293T-indE, Vero E6-TMPRSS2, and Vero-E2T see next chapter.

Cells were maintained in DMEM high glucose with 10% FBS + 1% Penicillin/ Streptomycin for general propagation or with 2% FBS + 1% Penicillin / Streptomycin for viral infection experiments. During the initial viral rescue, the JAK-I inhibitor Pyridone 6 (CAS 457081-03-7) was added to a final concentration of 2μM as well as the NFκB inhibitor QNZ (CAS 545380-34-5) at 20nM. HEK293T-indE received in addition Doxycycline (Merck, D5207) to a final concentration of 2 μg/mL for induction.

Cell line generation

HEK293T-E were generated by transfecting HEK293T with 2μg plasmid DNA containing the SARS-CoV-2 E gene under CMV promoter control in a pcDNA3.1 background containing a Hygromycin resistance gene. After transfection cells were put in DMEM containing 250μg/mL of Hygromycin. The selection was kept for two weeks and clones were generated by limiting dilution before E expression was tested by RT-qPCR. The clone that showed the highest RNA expression levels was kept for downstream application.

HEK293T-indE (HEK293T-E Tet:E-IRES-ORF6) are a derivative of HEK293T-E with a second-generation lentiviral vector generated with the pCW57-E-IRES-ORF6 (Addgene plasmid #80921) as a transfer vector. The vector codes for SARS-COV-2 E and ORF6 under a Tetracycline inducible promoter. After infection, cells were selected in DMEM containing 20μg/mL of blasticidin for two weeks. Cells were analyzed by RT-qPCR for E and ORF6 induction following doxycycline treatment (Extended Data Fig. 1c).

HEK293T-ACE2 were obtained by infecting the cells with a 2nd generation lentiviral vector with pHR-PGK_hACE2 (Addgene plasmid #161612) as a transfer vector. Cells were sorted for surface expression of ACE2 stained by Mouse anti-human ACE2 (R&D #FAB9332G).

Vero-E2T were generated by transfecting Vero E6 cells with 2μg of an equimolar plasmid mixture containing the SARS-COV-2 E/ORF6/ORF7a/ORF8 genes in individual plasmids all under the CMV promoter in a pcDNA3.1 background containing a Hygromycin resistance gene. After transfection cells were cultivated in DMEM containing 250μg/mL of Hygromycin. Human TMPRSS2 expression in Vero-E2T and in Vero E6 cells (Vero E6-TMPRSS2) was achieved by infecting the cells with a 2nd generation lentiviral vector pLEX307-TMPRSS2-blast (Addgene plasmid #158458) as a transfer vector. After infection cells were selected in DMEM containing 20μg/mL of blasticidin for two weeks and analyzed by RT-qPCR for transgene expression (Extended Data Fig. 1b).

Plasmids and lentivirus

The genes of interest from the Wuhan strain (B.1) were inserted into the pcDNA3.1 backbone under the control of the CMV promoter for expression. The all-in-E plasmid contains the SARS-CoV-2 genes E and ORF6 under control of an ELF1α promoter or an IRES sequence, respectively, followed by ACE2 and TMPRSS2 under PGK promoter control separated by a P2A cleavage site in a pcDNA3.1 background. The integrity of all plasmids was verified by Sanger sequencing.

The plasmids required for the generation of second-generation lentiviruses were obtained from Addgene. Lentiviruses were generated by transfecting HEK-293T cells with pCMVR8.74 (RRID:Addgene_22036), pMD2G (RRID:Addgene_12259), and pLEX307-TMPRSS2-blast (RRID:Addgene_158458) plasmids. The culture medium was changed 5 hours after transfection, supernatant was collected 24 hours later and filtered through a 0.22μm filter to remove cellular debris.

Genome reconstitution procedures for virus

Virus recovery was achieved as described in [22]. In brief PCR fragments (fr A-D) spanning the whole SARS-CoV-2 genome were amplified using the high-fidelity proofreading enzyme Q5® High-Fidelity DNA Polymerase (NEB, M0491L) in a 25 μL reaction volume using respective primers (Extended Data Fig. 1a and Extended Data Table 1). Fragment A contains the heterologous CMV promoter upstream of the 5' UTR and fragment D contains the poly(A) tail, HDV ribozyme, and SV40 termination signal downstream of the 3' UTR (Fig. 1a).

Cycling conditions were used as recommended by the manufacturer. Fragments were obtained using the following primer combinations: frA: CMV for + frA-frB rev; frB: frB-frA for + frB-frC rev; frC: frC-frB for + frC-frD rev; frD: frD-frC for + SV40 rev. DNA oligonucleotides used are listed in Extended Data Table 1.

12-30 reactions were pooled and purified by PCR column purification using QIAquick PCR purification kit (Qiagen, 28104). DNA concentration was measured by Nanodrop 1000 (Thermo Fisher) or Quantus (Promega, QuantiFluor® ONE dsDNA System, E4871). DNA was further purified by ethanol precipitation and the final concentration was adjusted to 1 μg/μL in nuclease-free water.

Equimolar ratios of frA, frB, frC, frD or ΔfrD and all-in-E plasmid were transfected into HEK293T-indE using jetPRIME® (Polyplus, cat. 101000001) as recommended by the manufacturer. 4-24h post-transfection, medium was changed to DMEM 2% FBS with addition of JAK-I inhibitor Pyridone 6 (CAS 457081-03-7) to a final concentration of 2μM as well as the NFκB inhibitor QNZ (CAS 545380-34-5) at 20 nM and 2 μg/mL Doxycycline and Vero-E2T were added for co-incubation. Every 3-4 days, the medium was exchanged. Screen for virus progeny production was done with SARS-CoV-2 antigen quick-test (Roche, 9901-NCOV-01G) (or CPE in E2T) and confirmed by RT-qPCR and FFA.

Virus propagation for viral stocks

For *wild-type* controls, clinical isolates Muc-1 (a Wuhan-1-type virus isolate, provided by G. Kochs, University of Freiburg, Germany (SARS-CoV_Muc)), BavPat1 (SARS-CoV-2 Germany/BavPat1/2020, GISAID accession EPI_ISL_406862, kindly provided by Bundeswehr Institute of Microbiology, Munich, Germany), XBB.1.5 (isolated from nasopharyngeal aspirates of human donors, who had given their informed consent (approval by Ethikkommission Nordwest- und Zentralschweiz #2022-00303)), synthetic SARS-CoV-2 (Wuhan-1, GenBank No. MT108784 [34]) or rCoV2 (recombinant Wuhan-1-type virus produced by genome reconstitution [22], were propagated in Vero E6 cells until CPE was observed.

For deletion mutants, viral particles produced by HEK293T-indE were further amplified in Vero-E2T cells, with additional trans-complementation of the all-in-E plasmid. Viral

propagation was observed and monitored by CPE and Antigen quick-tests [22] and confirmed by RT-qPCR and FFA.

Final viral stocks were harvested, filtered by 0.2 μm filters to remove cells and frozen in small aliquots. For each viral stock, the viral titer was determined by RT-qPCR and FFA or titration by plaque forming assay.

All work including infectious SARS-CoV-2 viruses and its recombinant variants was conducted in a biosafety level 3 facility at the Department Biomedicine within the University of Basel (approved by the Swiss Federal Office of Public Health (BAG) #A202850/3).

Standard plaque forming assay

Wild-type viral titers were determined by counting plaque-forming units (PFU) after incubation on susceptible cells. Vero E6 cells were seeded at a density of $4*10^6$ cells/96-well flat bottom plate in DMEM 2% FBS and incubated overnight at 37°C and 5% CO_2. Virus was added 1:10 onto the cell monolayer in duplicates or triplicates and serially diluted 1:2 or 1:3. Plates were incubated for 2 days at 34°C, 5% CO_2 until plaque formation was visible. For virus inactivation, 80µl of formaldehyde (15% w/v in PBS) (Merck, F8775) was added for 10 min to the cultures. After this period, fixative and culture medium were aspirated, and crystal violet (0.1% w/v) was added to each well and incubated for 5 min. Subsequently, the fixed and stained plates were gently rinsed several times with tap water and dried prior to analysis on a CTL ImmunoSpot® analyser.

RNA extraction for viral quantification and sequencing of viral stocks

Viral RNA was extracted using the automated Promega Maxwell RSC system (Promega, AS4500) using either the Maxwell® RSC Viral Total Nucleic Acid Purification Kit (Promega,

AS1330) or the Maxwell® RSC miRNA from the Tissue and Plasma or Serum Kit (Promega, AS1680).

Sanger sequencing

The region of interest was amplified using SuperScript™ IV One-Step RT-PCR System (Thermo Fisher, 12594100) with either F-D2 IDRA4 or F-26847 and R-29046 N. The integrity of the PCR product was checked on agarose gel and subsequently sent for Sanger sequencing (for primers see Extended Data Table 1) to evaluate genome regions affected by deletions/mutations (Microsynth, Switzerland).

Next-generation sequencing (NGS)

Viral RNA was converted to cDNA using cDNA Synthesis kit (biotechrabbit). cDNA was NGS sequenced using EasySeq SARS-CoV-2 WGS Library Prep Kit (NimaGen, SKU: RC-COV096) on an Illumina NextSeq 2000 system with a P1 flow cell (300 cycles). All NGS sequencing and raw data analysis was done by Seq-IT GmbH & Co. KG.

RT-qPCR quantification of viral and intracellular RNA

For detection of SARS-CoV-2 RNA, a primer and TaqMan probe set for ORF-1b (Extended Data Table 1) were used as described [35]. For the detection of SARS-CoV-2 E and TMPRSS2 an in-house primer / probe set was used (Extended Data Table 1). For normalization of mRNA expression GAPDH was used (Extended Data Table 1). For RT-qPCR Luna® Universal Probe One-Step RT-qPCR Kit (E3006E) was used according to manufacturer´s protocol. In brief Master Mix was set up: for one reaction 1 μL of each primer, 0.5 μL Probe, 10 μL of Luna Universal Probe One-Step Reaction Mix (2X), 1 μL of Luna WarmStart RT Enzyme Mix (20X) were mixed and brought to15 μL with nuclease free water. 15 μL of Master Mix were mixed with 5 μL RNA and amplified on ABI7500 fast cycler (ThermoFisher) using following cycling

conditions: 10 min 55 °C, 1min 95°C denaturation, followed by 40 cycles for 10 seconds at 95°C and 30 seconds at 58°C.

In vitro passaging for in vitro safety experiments

For viral passaging experiments, Vero E6 cells were infected with an MOI of 1 (based on FFU) for 3-4h with the *wild-type* or respective deletion candidate. The cells were then washed and fresh 2% DMEM medium was added. Every second day supernatant (SN) was passaged on freshly seeded Vero E6 (50% confluency). SNs for passage 1 (p1) and p2 were diluted 1:10, for all subsequent passages, SN was diluted 1:100. All collected passages p1 to p10 were subsequently passaged on Vero-E2T. On day 3 and day 6 post infection SN was sampled for RT-qPCR and images of cell cultures were taken with a Leica DM IL LED inverted microscope. All conditions were treated equally.

Biochemical procedures

For validation and comparison of vaccine candidate viruses, Vero E6-TMPRSS2 cells were infected with virus variants at an MOI of 0.1. 24h after infection, cells were washed twice with PBS before lysis in cold 140mM NaCl, 50mM Tris-HCL, 1% Triton-X100, 0,1% SDS, 0,1% sodium deoxycholate. supplemented with protease and phosphatase inhibitors (ThermoFisher, 1861281). Lysates were centrifuged for 10 min, 16'000g at 4°C and supernatants analyzed by Immunoblot. Signals were acquired using an image analyzer (Odyssey CLx, Licor).

Flow cytometry analysis

Transfection. Cells were transfected using JetPrime (Polyplus, 101000001) transfection reagent according to the manufacturer's protocol. Five hours after transfection, the culture

672 medium was replaced. In the case of THP-1 cells, only ¼ of the recommended amount of DNA
673 and reagents were used to avoid toxicity.
674 **Infection**. For cytometry experiments, all infections were conducted in DMEM supplemented
675 with 2% FBS using a multiplicity of infection (MOI) value of 0.1 based on FFU (focus forming
676 unit) data.
677 **Staining.** Cells were washed in PBS and stained with Zombie UV® Fixable Dead Cell Stain
678 (Biolegend), and rinsed once with PBS and blocked in blocking buffer (PBS with 50% FCS,
679 FcR Blocking Reagent 1:150 (Miltenyi Biotec) for 30 minutes at room temperature, followed
680 by incubation with antibodies against cell-surface molecules in staining buffer (PBS with 15%
681 FBS, FcR Blocking Reagent 1:1000) for 30 minutes at room temperature. Data were acquired
682 on the Aurora (Cytek, Amsterdam, Netherlands) equipped with 5 lasers (355, 405, 488, 561,
683 and 640 nm) and 60 channels (full spectrum cytometry), unmixed with SpectroFlo®, and
684 analysed with FlowJo 10.0.7 (TreeStar).
685
686 **Immunocytochemistry**
687 For detection of infectious vaccine viral particles (focus forming assay (FFA)), protein
688 expression analysis and surface labeling, Vero E6-TMPRSS2 cells grown on coverslips in 24-
689 well plates were infected with virus variants in 500 μL DMEM medium supplemented with 2%
690 FCS and 1% Penicillin/Streptomycin and incubated overnight. Cells were fixed with 4% PFA
691 in PBS for 10 min at room temperature, washed and subsequently stained. For FFA and
692 protein expression analysis, cells were blocked with 10% Normal Donkey Serum (Jackson
693 ImmunoResearch, 017-000-121) and 0.1% Triton X-100 at room temperature for 60 min
694 followed by incubation with primary antibodies for 60 min at room temperature or overnight at
695 4°C in 1% Normal Donkey Serum, 1% BSA and 0.3% Triton X-100 in PBS. Cells were washed
696 three times for 10 min with 0.1% BSA / PBS and incubated with fluorophore-coupled
697 secondary antibodies for 60 min at room temperature in 1% Normal Donkey Serum, 1% BSA

and 0.3% Triton X-100 in PBS. Cells were washed once with 0.1% BSA / PBS and washed three times with PBS before mounting on microscope slides using Fluoromount-G (SouthernBiotech, 0100-01). For surface labeling, cells were blocked with 5% milk powder in PBS at room temperature for 1hr and incubated with primary antibodies in 1% BSA / PBS overnight at 4°C. After 3 washes with PBS, fluorophore-coupled secondary antibodies in 1% BSA / PBS were applied for 60 min at room temperature washed three times with PBS before mounting on microscope slides. Phalloidin-iFluor488 or -iFluor555 was co-applied with secondary antibodies to label F-actin (Abcam, ab176753 and ab176756 resp.). Hoechst 33342 dye (Merck, B2261) was co-applied during washing at a final concentration of 0.5 μg/mL for nuclear staining.

Images for FFA were acquired on a bright-field microscope (Nikon Ti2 equipped with a Photometrics 95B camera, Nikon NIS AR software), using a 20x Plan-Apochromat objective (numerical aperture 0.75) and were then processed in Fiji and Omero. For quantification of infected foci, images were analyzed with QuPath. Images for protein expression and surface labeling were acquired on an inverted spinning-disk confocal microscope (Nikon Ti2 equipped with a Photometrics Kinetix 25mm back-illuminated sCMOS, Nikon NIS AR software), using 40x and 100x Plan-Apochromat objectives (numerical aperture 0.95 and 1.45 respectively) and were then processed in Fiji and Omero.

Electron microscopy

Viral particles were fixed in 1% glutaraldehyde (Thermo Scientific, 233281000). A 4 μL aliquot of sample was adsorbed onto holey carbon-coated grid (Lacey, Tedpella, USA), blotted with Whatman 1 filter paper and vitrified into liquid ethane at -180°C using a Leica GP2 plunger (Leica microsystems, Austria). Frozen grids were transferred onto a Talos 200C Electron microscope (FEI, USA) using a Gatan 626 cryo-holder (GATAN, USA). Electron micrographs were recorded at an accelerating voltage of 200 kV using a low-dose system (40 e-/Å2) and

keeping the sample at -175°C. Defocus values were -2 to 3 μm. Micrographs were recorded on 4K x 4K Ceta CMOS camera.

Animal immunization and analysis

ΔE^G immunization. Eight hamsters were intranasally inoculated with 100 μL of ΔE^G virus stock ($3.5*10^3$ FFU, Extended Data Fig. 4b,d) at day 0 and boosted with the same dose at day 21. Four hamsters were inoculated with 100 μL of supernatant from uninfected cells and therefore served as sham vaccinated controls. The three direct contact animals were co-housed with ΔE^G immunized animals, but were separated for 24 hours just prior to immunizations and challenge, respectively. Nasal washing samples were taken at day -2, 3, 7, 24, 28, 36, 37, 39, 43 and 47 days post immunization (dpim), by applying 200 μL of PBS into each nostril and collecting the reflux under short isoflurane inhalation anesthesia. Serum samples were taken by puncturing the *V. saphena* at 19 and 33 dpim for serological evaluation. At 35 dpim eight ΔE^G immunized animals and four sham vaccinated control animals (intranasally inoculated with filtered medium of non-infected cells) were challenged by intranasal inoculation using $10^{2,5}$ $TCID_{50}$/animal of SARS-CoV-2 virus (Wuhan-1, GenBank No. MT108784 [34]) in a 70 μL volume (calculated from back-titration). Five days post challenge (dpc), five ΔE^G immunized hamsters and the sham vaccinated control hamsters were sacrificed and sera or organ samples from upper and lower respiratory tract were collected during necropsy. 14 dpc three ΔE^G immunized hamsters and three contact animals were euthanized and serum sample as well as organ samples from upper and lower respiratory tract were collected during necropsy.

ΔE^G68 immunization. Twelve hamsters were intranasal inoculated with 100 μL of ΔE^G68 virus stock ($2.4*10^5$ FFU, Extended Data Fig. 4a,c) at day 0 and boosted with the same dose at day 21. Six direct contact animals were co-housed with ΔE^G68 immunized animals, but were separated for 24 hours prior to immunizations and challenge infection, respectively.

Nasal washing samples were taken at dpim -2, 3, 7, 24, 28, 36, 37, 38, 41 (dpc1), 42 (dpc2), 44 (dpc4) and 48 (dpc8) by applying 200μL of PBS in each nostril and collecting the reflux under short isoflurane inhalation anesthesia. Serum samples were taken by puncturing the *V. saphena* at 19 and 33 dpim for serological evaluation. At 35 dpim the ΔE^G68 immunized animals were inoculated using a miscalculated low dosage of SARS-CoV-2 virus (Wuhan-1, GenBank No. MT108784 [34]) with less than 1 $TCID_{50}$/animal. The viral genome copies in this misdiluted inoculum were determined by RT-qPCR (RNA-dependent RNA polymerase (IP4) as target [36]) with a Ct-value of 35.64, representing 1089 genome copies/mL. With this highly diluted inoculum, we were unable to perform an endpoint titration and to initiate a productive infection when 70 μL of pure inoculum were applied to Vero E6 cells (0.32 cm^2, n=7). Additionally, nasal washing samples were taken from all animals on the first three days after inoculation and were all negative by RT-qPCR (Extended Data Table 2). Therefore, a second challenge infection was performed with the same animals at 41 dpim applying 70 μL with $10^{2.3}$ $TCID_{50}$/animal (Wuhan-1, GenBank No. MT108784 [34]), calculated from back-titration. Five days post challenge infection, six ΔE^G68 immunized hamsters were euthanized and serum samples as well as organ samples from the upper and lower respiratory tract were collected during necropsy. 14 dpc six ΔE^G immunized hamsters and their respective six matching contact animals were euthanized and serum sample as well as organ samples from upper and lower respiratory tract were collected during necropsy.

RNA analysis of hamster samples. RNA from nasal washings and organ samples was extracted using the NucleoMag® VET Kit (Macherey-Nagel, Düren, Germany) in combination with a Biosprint 96 platform (Qiagen, Hilden, Germany). Viral RNA genomes were detected and quantified by real-time RT-qPCR on a BioRad real-time CFX96 detection system (BioRad, Hercules, USA). The target sequence for amplification was viral RNA-dependent RNA polymerase (IP4) [27,36]. Genome copies per mL sample were calculated based on a quantified standard RNA, where absolute quantification was done by the QX200 Droplet Digital PCR

776 System in combination with the 1-Step RT-ddPCR Advanced Kit for Probes (BioRad,
777 Hercules, USA). The detection limit was calculated to be 1000 copies per reaction.
778 **ELISA.** Serum samples were analysed using an indirect multispecies ELISA against SARS-
779 CoV-2 RBD [37]. Briefly, RBD coated plates or those treated with coating buffer-only were
780 blocked with 5% skim milk in phosphate-buffered saline, pH 7.5. Serum samples were
781 incubated on the coated and uncoated wells for 1 h at room temperature. Using a multi-species
782 conjugate (SBVMILK; obtained from ID Screen® Schmallenberg virus Milk Indirect ELISA;
783 IDvet) diluted 1/80 for 1 h at room temperature detection was performed after the addition of
784 tetramethylbenzidine (TMB) substrate (IDEXX) at a wavelength of 450 nm. After each step,
785 the plates were washed three times with Tris-buffered saline with Tween 20. For readout,
786 absorbances were calculated by subtracting the optical density (OD) measured on the
787 uncoated wells from the values obtained from the protein-coated wells for each respective
788 sample. Reproducibility was confirmed and normalization was achieved by reference to
789 negative and positive sera samples.
790 IFN and IL-10 were measured in homogenized hamster organs by ELISA. Organ samples of
791 about 0,1 cm^3 size from hamsters were homogenized in a 1 mL mixture composed of equal
792 volumes of Hank's balanced salts MEM and Earle's balanced salts MEM (containing 2 mM L-
793 glutamine, 850 mg/L NaHCO3, 120 mg/L sodium pyruvate, and 1% penicillin–streptomycin)
794 at 300 Hz for 2 min using a Tissuelyser II (Qiagen) and were then centrifuged to clarify the
795 supernatant. 50μL of this homogenate was then used as a sample according to the
796 manufacturer's instruction with the Hamster IFNγ (Assaygenie #HMFI0010) and Hamster IL-
797 10 ELISA Kit (Assaygenie #HMFI0003) for IFNγ and IL-10 respectively.
798 **Neutralization Assay.** To evaluate specifically the presence of virus-neutralizing antibodies
799 in serum samples we performed a virus neutralization test. Sera were pre-diluted (starting
800 dilution from 1/16 to 1/512) with Dulbecco's modified Eagle's medium (DMEM) in a 96-well
801 deep well master plate. 100μL of this pre-dilution was transferred into a 96-well plate. A log2

dilution was conducted by passaging 50 μL of the serum dilution in 50 μL DMEM, leaving 50 μL of sera dilution in each well. Subsequently, 50 μL of SARS-CoV-2 (BavPat1) virus dilution (100 $TCID_{50}$/well) was added to each well and incubated for 1 h at 37 °C. Lastly, 100 μL of trypsinized Vero E6 cells (cells of one confluent T-175 flask per 100 mL) in DMEM with 1% penicillin/streptomycin supplementation was added to each well. After 72 h incubation at 37 °C, the cells were evaluated by light microscopy for a specific CPE. A serum dilution was counted as neutralizing in the case no specific CPE was visible and is given as neutralizing dose 100 (ND100). The virus titer was confirmed by virus titration; positive and negative serum samples were included. Tests were performed in 3 technical replicates and average values were used to calculate the 100% neutralizing dose with the Kerber formula: (-log2) = a/b + c ((a) cell culture wells without virus replication, (b) number of cell culture wells per sera dilution, (c) -log2 of pre-dilution of the sera/yolk sample).

Pathology. For histopathology, the left lung lobe was processed as described [38]. The left lung lobe was carefully removed, immersion-fixed in 10% neutral-buffered formalin, paraffin-embedded, and 2- to 3-µm sections were stained with hematoxylin and eosin (HE). Consecutive sections were processed for immunohistochemistry (IHC) used according to standardized procedures of avidin-biotin-peroxidase complex (ABC)-method [39]. Briefly, endogenous peroxidase was quenched on dewaxed lung slides with 3% hydrogen peroxide in distilled water for 10 minutes at room temperature (RT). Antigen heat retrieval was performed in 10mM citrate buffer (pH 6) for 20 minutes in a pressure cooker. Nonspecific antibody binding was blocked for 30 minutes at RT with goat normal serum, diluted in PBS (1:2). A primary anti-SARS-CoV nucleocapsid protein antibody was applied overnight at 4°C (1:3000), the secondary biotinylated goat anti-mouse antibody was applied for 30 minutes at room temperature (Vector Laboratories, Burlingame, CA, USA, 1:200). Color was developed by incubation with ABC solution (Vectastain Elite ABC Kit; Vector Laboratories), followed by exposure to 3-amino-9-ethylcarbazole substrate (AEC, Dako, Carpinteria, CA, USA). The

sections were counterstained with Mayer's hematoxylin. As a negative control, consecutive sections were labeled with an irrelevant antibody (M protein of Influenza A virus, ATCC clone HB-64). An archived control slide from a SARS-CoV-2-infected Syrian hamster was included in each run. All slides were scanned using a Hamamatsu S60 scanner and evaluated using the NDPview.2 plus software (Version 2.8.24, Hamamatsu Photonics, K.K. Japan) by a trained (TB) and reviewed by a board-certified pathologist (AB), blind to treatment. The lung was evaluated using a 500 × 500 µm grid, and the extent of pneumonia-associated consolidation was recorded as the percentage of affected lung fields. We examined for the presence of SARS-CoV-2-characteristic lesions as given in Extended Data Table 3. Following IHC the distribution of virus antigen was graded on an ordinal scale with scores 0 = no antigen, 1 = focal, affected cells/tissue <5% or up to 3 foci per tissue; 2 = multifocal, 6%–40% affected; 3 = coalescing, 41%–80% affected; 4 = diffuse, >80% affected. The target cell was identified based on morphology.

Antibodies

The following antibodies were used in this study: mouse monoclonal anti-β-actin (Cell Signaling Technology; 3700; RRID: AB_2242334; LOT# 20), rabbit polyclonal anti-SARS-CoV-2 nsp2 (GeneTex; GTX135717; RRID: AB_2909866; LOT# B318853), rabbit polyclonal anti-SARS-CoV Nucleocapsid protein (Rockland; 200-401-A50; RRID:AB_828403), mouse monoclonal anti-SARS-CoV-2 Nucleocapsid protein (4F3C4, gift from Sven Reiche [40]), sheep polyclonal anti-SARS-CoV-2 ORF3a [41], rat monoclonal anti-SARS-CoV-2 ORF6 (8B10, gift from Yoichi Miyamoto [42]), rabbit polyclonal anti-SARS-CoV-2 ORF8 (Novus Biologicals; NBP3-07972; LOT# 25966-2102), mouse monoclonal anti-SARS-CoV-2 Spike protein (4B5C1, gift from Sven Reiche).

Fluorophore-conjugated secondary antibodies were from Jackson ImmunoResearch (Cy3 donkey anti-rat #712-165-153, Cy3 donkey anti-mouse #715-165-151, Cy5 donkey anti-rabbit

#711-175-152, Cy5 donkey anti-mouse #715-175-511), Li-Cor (IRDye 680RD donkey anti-mouse #926-68072, IRDye 680RD goat anti-rabbit #926-68071, IRDye 680RD goat anti-rat #926-68076) and Invitrogen (Alexa Fluor 647 donkey anti-mouse #A31571, Alexa Fluor 680 donkey anti-sheep #A21102).

Flow cytometry antibodies -all anti-human- were from Miltenyi REAfinity™ (VioBlue™ anti CD44 #130-113-344, VioGreen™ anti HLA-ABC #130-120-436, PerCP-Vio-700 anti CD59 #130-128-812, PE-Vio®770 anti CD275 (B7-H2) #130-116-805, APC anti CD70 # 130-130-100), Biolegend (Brilliant Violet 711 anti CD80 #305236, Alexa Fluor® 700 anti HLA-DR #307626) and R&D (mouse monoclonal anti-hACE2 #FAB9332G).

Statistical analysis

Data were analyzed using GraphPad Prism 9 software. Sample sizes were chosen based on previous experiments and literature surveys. No statistical methods were used to pre-determine sample sizes. Acquisition and analysis of lung pathology were done by an investigator blinded to the condition. Appropriate statistical tests were chosen based on sample size and are indicated in individual experiments.

Materials availability

This study has generated plasmids, which will be deposited to Addgene.

Data availability

All sequencing data will be deposited at NCBI.

Acknowledgements

We are grateful to Laurent Perez and Christian Münz for helpful comments on the manuscript. The authors thank the BioEM lab and Mohamed Chami of the Biozentrum, University of Basel, for their support with electron microscopy and the DBM Microscopy Core Facility for support with image acquisition and analysis. We thank Sven Reiche (FLI, Greifswald, GER) for the generous provision of monoclonal anti-S and anti-N antibodies, which were obtained through the EU H2020 project EVA-GLOBAL, project #871029, and Yoichi Miyamoto (Natl. Inst. Biomed. Innovation, Health and Nutrition, Osaka, J) for the anti-ORF6 antibody. We are thankful to Mareen Grawe, Robin Brandt and the animal caretakers for their essential help. We thank G. Kochs, Freiburg, GER for providing the SARS-CoV-2 Wuhan isolate and Martin Daeumer, Alex Thielen (Seq-It GmbH, Kaiserslautern, GER) and Adrian Egli & team (USB, Basel, CH) for expert NGS support. pCMVR8.74 and pMD2.G were a gift from Didier Trono (RRID:Addgene_12259), pLEX307-TMPRSS2-blast was a gift from Alejandro Chavez & Sho Iketani (RRID:Addgene_158458). pHR_PGK-hACE2 was a gift from Brad Rosenberg (RRID:Addgene_161612). Vero E6 cells and synthetic SARS-CoV-2 virus (Wuhan-1, GenBank No. MT108784) were kindly provided by V. Thiel. Graphical symbols were created with BioRender.com. **Funding:** This research was co-funded through a federal project grant through the Innosuisse project #52533.1 IP-LS and by RocketVax AG, Basel, CH, through a project grant with the University Hospital Basel/Canton Basel Stadt, CH, granted to TK. The funders did not influence the experimental design or the conduct of work.

Author contributions

This work was jointly conceived by M.J.L., F.O., D.H., M.B., C.M., and T.K., experimental procedures were performed by M.J.L, F.O., D.H., J.S., E.K., N.J.H., L.U., Y.Z., C.W., L.U., D.Ho., A.B., T.B., and C.L., data analysis was conducted by M.J.L., F.O., D.H., A.B., T.B., and J.S.. The manuscript was jointly written by M.J.L, F.O., D.H., and T.K., with editing provided

902 by J.S., D.Ho., M.B. and C.M.. All authors have read and approved the final version of the
903 manuscript.
904
905 **Competing interests**
906 VC owns shares of RocketVax AG, Basel, CH. The other authors declare no competing
907 interests. A patent application (no. WO 203/036947 A1) has been filed on the topic of this
908 vaccine.

Inventory of Extended Data:

1) Extended Data Figures:

Extended Data Fig. 1: Production and *in vitro* characterization of SCVs (addition to Fig. 1)

Extended Data Fig. 2: Immunomodulation by E, ORF6 and ORF8 proteins (addition to Fig. 2)

Extended Data Fig. 3: Phylogenetic analysis of ORF8 mutations (addition to Fig. 2)

Extended Data Fig. 4: SCV quantification and pathology analysis (addition to Fig. 3 and 4)

2) Extended Data Tables:

Extended Data Table 1. Methods supplement

Extended Data Table 2. qPCR evaluation $\Delta E^{G}68$ vaccinated animals (addition to Fig. 3)

Extended Data Table 3. Lung pathology score sheet (addition to Fig. 4, Extended Data Fig. 4)

Extended Data Table 4. Neutralization data (addition to Fig. 3 and 4)

Extended Data Fig. 1: Production and in vitro characterization of SCVs

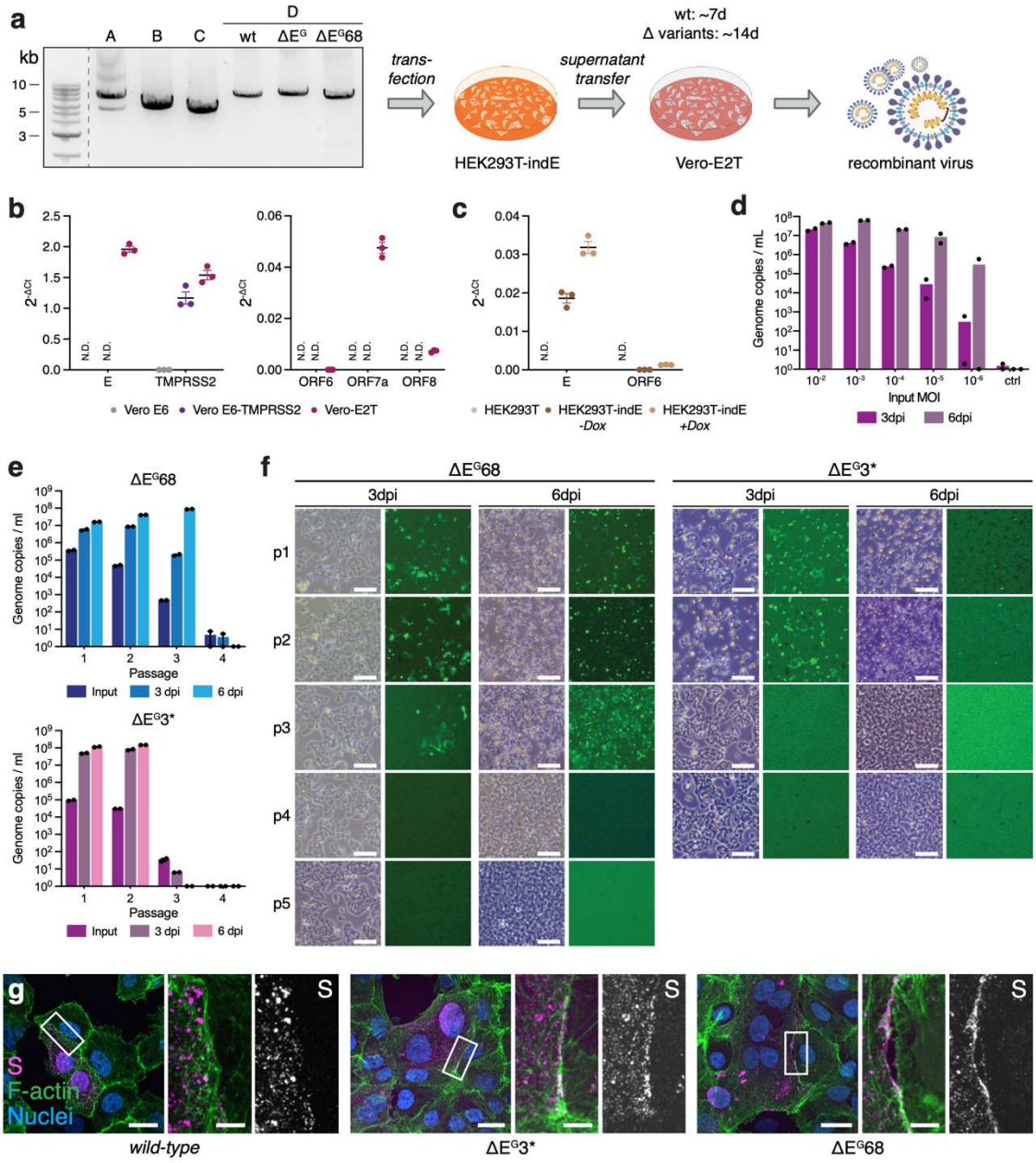

922

Extended Data Fig. 1: Production and *in vitro* characterization of SCVs (addition to Fig. 1)

a, Scheme showing virus production. Representative DNA gel showing PCR products of the four fragments A, B, C and D (for D: *wild-type* (wt), ΔE^G and $\Delta E^G 68$) amplified from plasmids encoding individual fragments A-D of SARS-CoV-2 followed by transfection of HEK293T-indE cells for spontaneous genome reconstitution and supernatant transfer onto Vero-E2T cells for virus harvest.

b, Quantification of transgenes by RT-qPCR for expression of *E* and *TMPRSS2* (left panel) or *ORF6*, *ORF7a* and *ORF8* (right panel) relative to *GAPDH* in Vero E6, Vero E6-TMPRSS2 or Vero-E2T cells, non-detectable signal annotated with N.D. (n=3 independent mRNA isolations).

c, Quantification of transgenes by RT-qPCR for expression of *E* and *ORF6* relative to *GAPDH* in HEK293T or HEK293T-indE treated +/- doxycycline for 48h, non-detectable signal annotated with N.D. (n=3 independent mRNA isolations).

d, Infection of complementing Vero-E2T cells with $\Delta E^G 3^*$ at different MOIs and analysis by RT-qPCR of the *ORF1b NSP14* regions normalized to external SARS-CoV-2 standards after 3- and 6-days post infection (n=2 infected cultures).

e, Analysis of supernatants from Vero E6 passaging experiment on complementing Vero-E2T cells by RT-qPCR, passages 1-4 from $\Delta E^G 68$ and $\Delta E^G 3^*$ were analyzed at timepoints 0 (Input) or 3- and 6-days post infection (n=2 technical replicates).

f, Images of infected, complementing Vero-E2T cells with supernatants from passaging experiment (p1-p4 or p5) after 3- and 6-days post infection for $\Delta E^G 68$ and $\Delta E^G 3^*$. Images show bright field view on the left, expression of eGFP on the right.

g, Surface labeling of S (magenta), F-actin (green), and nuclei (blue) in Vero E6-TMPRSS2 cells infected with *wild-type* SARS-CoV-2, $\Delta E^G 3^*$, or $\Delta E^G 68$.

948 Mean and S.E.M, scale bar is 200μm in (**f**) and 20μm for overview and 5μm for ROI images

949 in (**g**).

Extended Data Fig. 2: Immunomodulation by E, ORF6 and ORF8 proteins

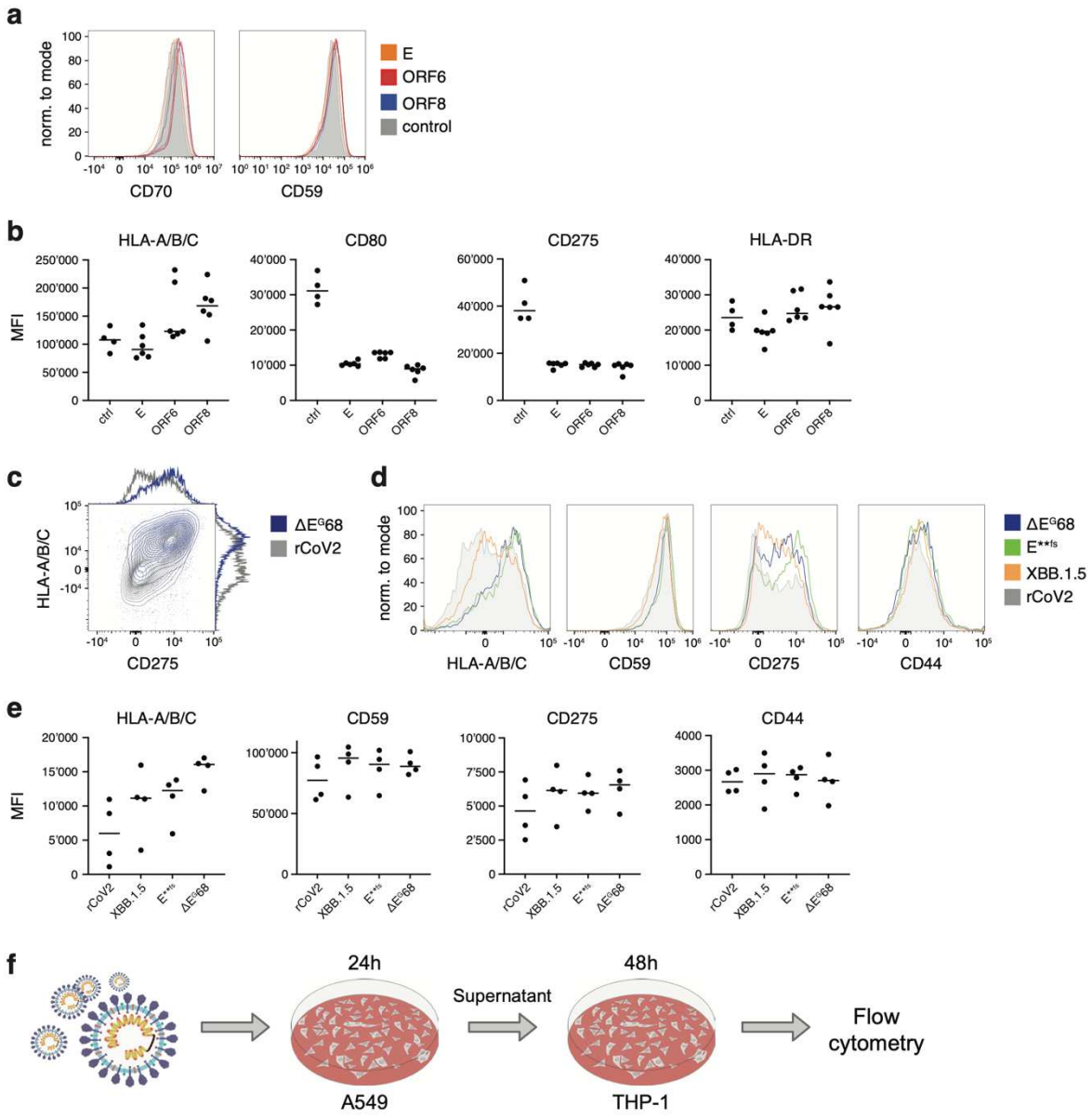

950

Extended Data Fig. 2: Immunomodulation by E, ORF6 and ORF8 proteins (addition to Fig. 2)

a,b, Modulation after transfection: **a,** Flow cytometry staining for surface expression of CD70 and CD59 on THP-1, 48h after transfection with plasmids coding for ORF6, ORF8, or Envelope proteins, compared with control transfection. **b,** Median fluorescence intensity of HLA-A/B/C, CD275, CD80, and HLA-DR corresponding to Fig. 3.

c-e, Modulation after infection: HEK293T-ACE2 cells were infected with rCoV2, E^{**fs}, $\Delta E^{G}68$, or XBB.1.5 SARS-CoV-2 virus (MOI = 0.1) for 24h. **c,** Contour plot comparing the expression of HLA-A/B/C and CD275 on the HEK-293T. **d,** Histogram showing the expression of HLA-A/B/C CD59, CD275, and CD44 on HEK-293T. **e,** Median fluorescence intensity of HLA-A/B/C, CD59, CD275, and CD274 for the different replicates of the experiment.

f, Method representation: Respective supernatants from the above-mentioned infections were applied on THP-1 for 48h before surface staining and analysis (Fig. 3).

Extended Data Fig. 3: Phylogenetic analysis of ORF8 mutations

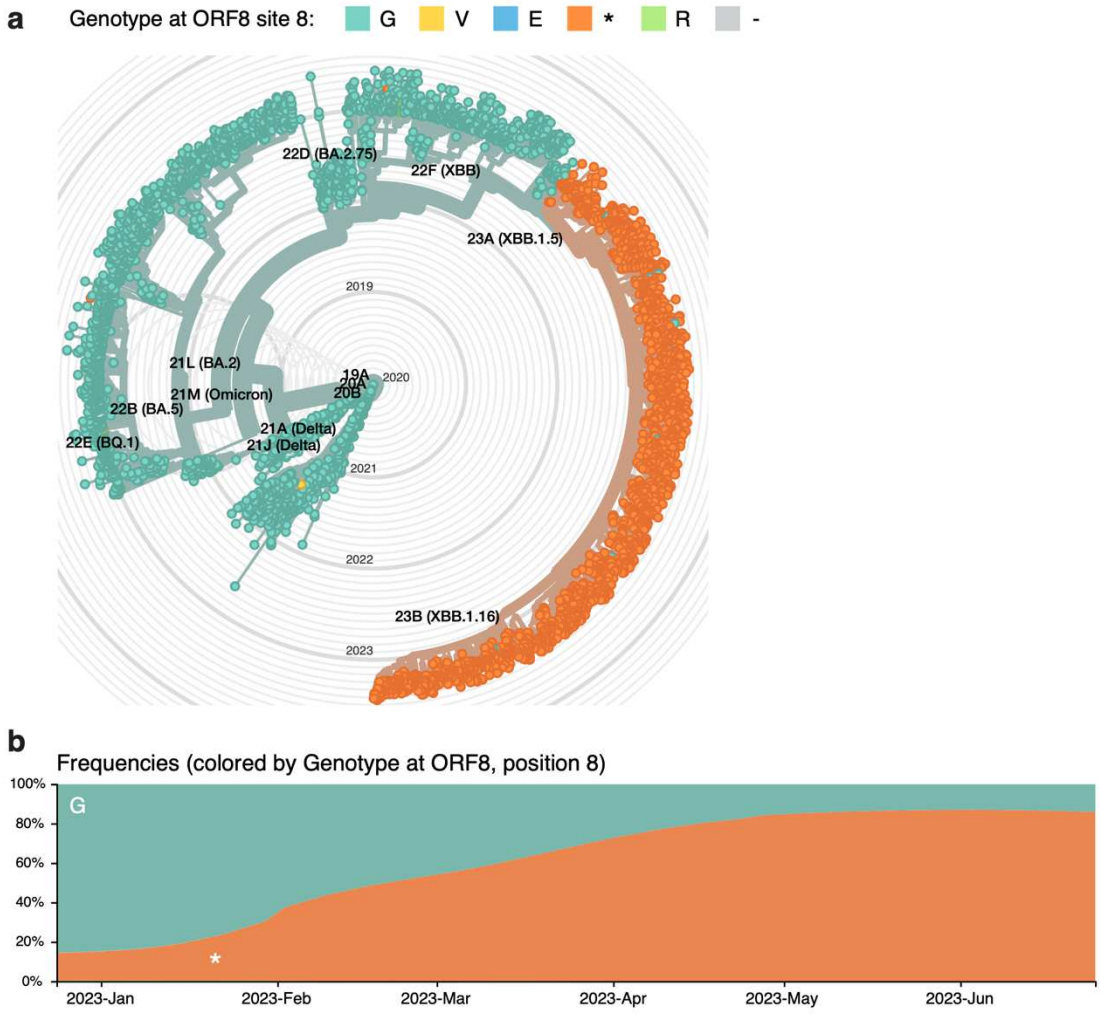

964

Extended Data Fig. 3: Phylogenetic analysis of ORF8 mutations (addition to Fig. 2)

a, Circular phylogenetic tree of SARS-CoV-2 virus isolates from the currently ongoing SARS-CoV-2 pandemic. Shown are 3858 representative genomes from GISAID color coded for amino acid 8 of ORF8 and the Clade name next to each tree branch. Isolines show time of isolation from the initial occurrence of SARS-CoV-2. The legend next to the plot shows the amino acid color code. The variant of concern XBB.1.5 delineates from all other variants with a premature stop codon at position 8 of ORF8 (orange, n=1222). Data update from 2023-06-24.

b, Frequency of SARS-CoV-2 isolates from (**a**) having a Glycine (G) or a stop codon (*) at position 8 of ORF8, shown over the period of 6 months (Jan 2022 – June 2023).

Source: https://nextstrain.org/ncov/gisaid/global/6m?c=gt-ORF8_8&l=radial

Extended Data Fig. 4: SCV quantification and pathology analysis

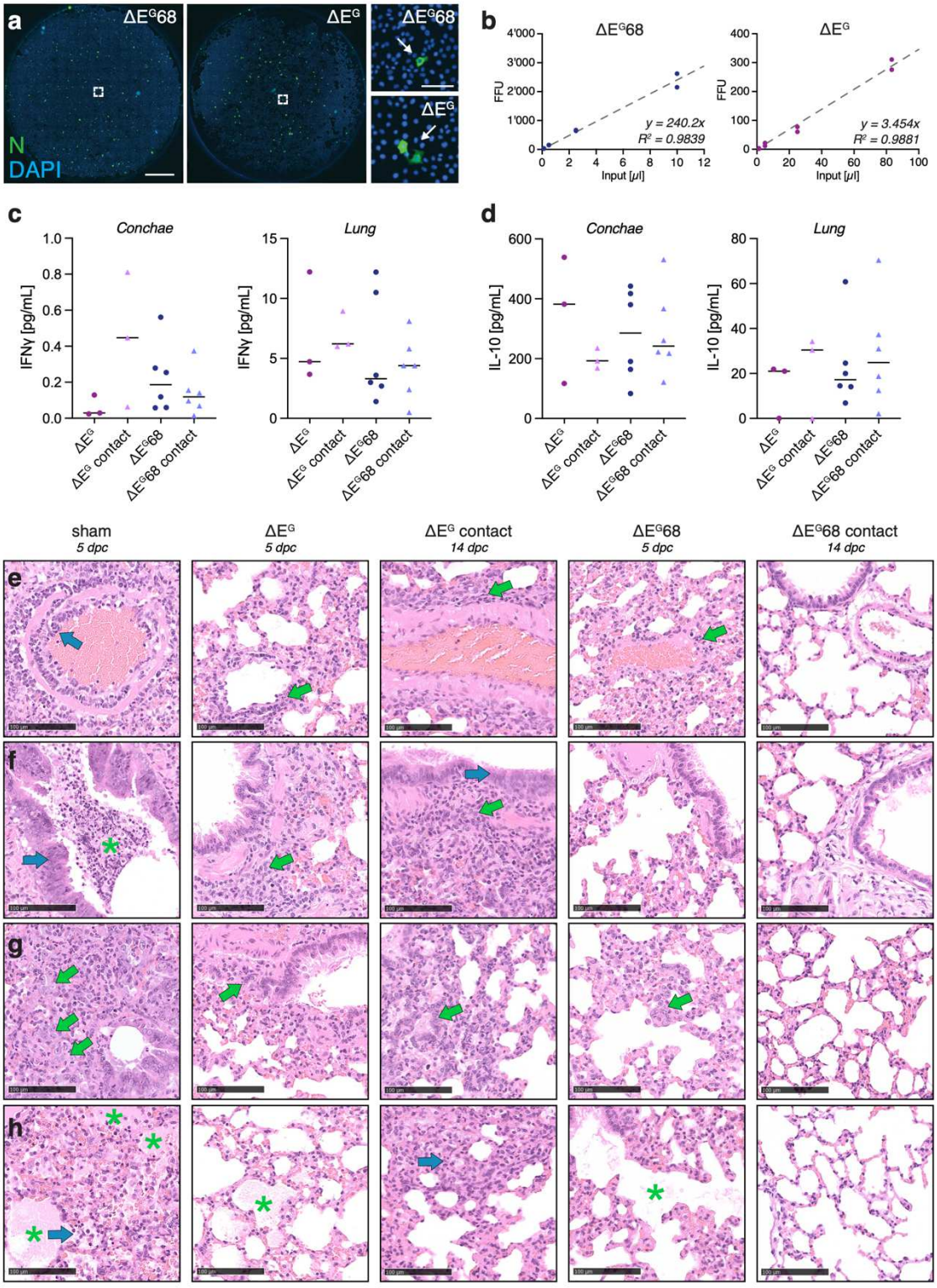

976

Extended Data Fig. 4: SCV quantification and pathology analysis (addition to Fig. 3 and 4)

a, Representative example of infected cells used to quantify viral titers of SCVs on coverslips in a 24-well culture dish for $\Delta E^G 68$ and ΔE^G in Vero E6-TMPRSS2 cells, detection of N shown in green, nuclei are stained with Hoechst (blue). Left: overview images, right: region of interest images showing individual infected cells as indicated.

b, Titration of $\Delta E^G 68$ and ΔE^G and quantification by FFA (n=2). Linear fit and correlation indicated for determination of SCV titers used to inoculate Syrian hamsters.

c,d, Cytokine levels in conchae and lungs of $\Delta E^G 68$ and ΔE^G vaccinated hamsters or contact groups 14 dpc, ELISA for IFNγ (**c**) and IL-10 (**d**).

e, Slight perivascular immune cell infiltrates (green arrow, $\Delta E^G 68$, ΔE^G or contact ΔE^G group), severe vasculitis (blue arrow, sham group), or no lesion ($\Delta E^G 68$ contact group).

f, Mild peribronchial infiltrates (green arrow, ΔE^G or contact ΔE^G group) and severe necrotizing bronchitis (green asterisk, sham group) as well as bronchial epithelial hypertrophy/hyperplasia (blue arrow, sham or contact ΔE^G group), or no lesion ($\Delta E^G 68$ and $\Delta E^G 68$ contact group).

g, Type-II pneumocyte hyperplasia (green arrow, oligofocal in $\Delta E^G 68$, ΔE^G or contact ΔE^G group, multifocal for sham group), or no lesion ($\Delta E^G 68$ contact group).

h, Alveolar edema (green asterisk), oligofocal ($\Delta E^G 68$ or ΔE^G group) and multifocal (sham group) as well as alveolar inflammatory infiltrates admixed with cellular necrotic debris (blue arrow, sham or contact ΔE^G group), or no lesion ($\Delta E^G 68$ contact group).

Scale bar is 2mm and 100μm in (**a**) (overview and ROI images resp.), and 100 μm in (**e-h**).

Extended Data Table 1. Methods supplement

Oligonucleotide primers and qPCR probes.

Name (gene / fragment)	Sequence
E-Sarbeco for	ACA GGT ACG TTA ATA GTT AAT AGC GT
E-Sarbeco rev	ATA TTG CAG CAG TAC GCA CAC A
E-Sarbeco probe	FAM-ACA CTA GCC ATC CTT ACT GCG CTT CG-BHQ-1
nCoV IP4-14059 for	GGT AAC TGG TAT GAT TTC G
nCoV IP4-14146 rev	CTG GTC AAG GTT AAT ATA GG
nCoV IP4-14084 probe	FAM-TCA TAC AAA CCA CGC CAG G-BHQ-1
β-actin for	CAG CAC AAT GAA GAT CAA GAT CAT C
β-actin rev	CGG ACT CAT CGT ACT CCT GCT T
β-actin probe	HEX-TCG CTG TCC ACC TTC CAG CAG ATG T-BHQ1
ORF1b for	TGG GGT TTT ACA GGT AAC CT
ORF1b rev	AAC ACG CTT AAC AAA GCA CTC
ORF1b probe	FAM-TAG TTG TGA TGC AAT CAT GAC TAG-BHQ1
Envelope for	GCG TAC TTC TTT TTC TTG CTT TCG
Envelope rev	TTG CAG CAG TAC GCA CAC AA
Envelope probe	FAM-CAC TAG CCA TCC TTA CTG CGC TTC GA-BHQ1
ORF6 for	GCA GAG ATA TTA CTA ATT ATT ATG AGG ACT TTT A
ORF6 rev	TCT CCA TTG GTT GCT CTT CA
ORF6 probe	FAM-TCC ATT TGG AAT CTT GAT TAC ATC ATA AAC CTC A-BHQ1
ORF7a for	CGA GGG CAA TTC ACC ATT TC
ORF7a rev	CGT GTT TTA CGC CGT CAG GA
ORF7a probe	FAM-TGC ACT GAC TTG CTT TAG CAC TCA ATT TGC-BHQ1
ORF8 for	CCT TTA ATT GAA TTG TGC GTG GA
ORF8 rev	CCC AAT TTA GGT TCC TGG CAA
ORF8 probe	FAM-TGA GGC TGG TTC TAA ATC ACC CAT TCA GT-BHQ1
TMPRSS2 for	CTC TAA CTG GTG TGA TGG CG
TMPRSS2 rev	TGC CAG GAC TTC CTC TGA G
TMPRSS2 probe	FAM-CGG ACC AAA CTT CAT CCT TCA GG-BHQ1
GAPDH for	GAA GGT GAA GGT CGG AGT C
GAPDH rev	GAA GAT GGT GAT GGG ATT TC
GAPDH probe	FAM-CAA GCT TCC CGT TCT CAG CC-BHQ1
CMV for	CGA TGT ACG GGC CAG ATA TAC G
frA-frB rev	GTG TTA TTA AAT AGA AAA TAG CAG CAA CAA AAA GGA ACA CAA GTG TAA CTT TAA TTA ACT GCT TCA ACC
frB-frA for	GCA CTT AAG GGT GGT AAA ATT GTT AAT AAT TGG TTG AAG CAG TTA ATT AAA GTT ACA CTT GTG TTC C
frB-frC rev	AAA CTG TCT ATT GGT CAT AGT ACT ACA GAT AGA GAC ACC AGC TAC GGT GCG AGC TCT ATT CTT TGC AC
frC-frB for	TAT AAC TCA AAT GAA TCT TAA GTA TGC CAT TAG TGC AAA GAA TAG AGC TCG CAC CGT AGC TGG TG
frC-frD rev	ATC ACC AAT CAA AGT TGA ATC TGC ATC AGA GAC AAA GTC ATT AAG ATC TGA GTC GAC AAG CAG CG

Name (gene / fragment)	Sequence
frD-frC for	TAC AGC TGT TTT AAG ACA GTG GTT GCC TAC GGG TAC GCT GCT TGT CGA CTC AGA TCT TAA TGA CTT TGT C
SV40 rev	GCG GCC GCC AGA CAT GAT AAG
D2 for	GGA ACT GTA ACT TTG AAG CAA GGT G
29046 N rev	CGA CGT TGT TTT GAT CGC GCC C
26847 for	GGA ACC AAT TTA TGA TGA ACC GAC G
26526 SARS2 La for	GCA GAT TCC AAC GGT ACT ATT ACC
M 574 for	TGT GAC ATC AAG GAC CTG CC

1001

Extended Data Table 2. qPCR evaluation ΔE^{G}68 vaccinated animals (addition to Fig. 3)

Envelope qPCR analysis of nasal washings of ΔE^{G}68 vaccinated animals to test for *wild-type* reversion in vaccinated animals or contact animals at different time points (dpim 0, 3, 7, and 24) and IP4 qPCR analysis of nasal washings of ΔE^{G}68 vaccinated and contact animals after miscalculated challenge infection on days 1, 2, and 3 after challenge.

Values are Ct values measured with SARS-CoV-2 Envelope, IP4, or beta-actin specific primer/probe sets. For negative controls, plain PBS was used and processed along with nasal washings. Inoculum of miscalculated challenge: Ct=35.64, 1089 gc/ml (N.D.: not detected).

	ID	dpim 0		dpim 3		dpim 7		dpim 24			dpc 1		dpc 2		dpc 3	
		E	β-act	E	β-act	E	β-act	E	β-act		IP4	β-act	IP4	β-act	IP4	β-act
$\Delta E^{G}68$	1	N.D.	35.71	N.D.	31.87	N.D.	32.17	N.D.	30.58		N.D.	33.84	N.D.	31.60	N.D.	26.96
$\Delta E^{G}68$	2	N.D.	34.25	N.D.	31	N.D.	30.57	N.D.	32.45		N.D.	30.65	N.D.	30.70	N.D.	28.79
$\Delta E^{G}68$	3	N.D.	N.D.	N.D.	31.35	N.D.	30.19	N.D.	29.25		N.D.	32.11	N.D.	32.34	N.D.	29.53
$\Delta E^{G}68$	4	N.D.	34.66	N.D.	29.87	N.D.	32.17	N.D.	30.52		N.D.	30.75	N.D.	32.38	N.D.	30.94
$\Delta E^{G}68$	5	N.D.	31.64	N.D.	31.92	N.D.	30.13	N.D.	30.71		N.D.	29.68	N.D.	31.82	N.D.	31.09
$\Delta E^{G}68$	6	N.D.	33.29	N.D.	33.36	N.D.	32.65	N.D.	32.82		N.D.	30.96	N.D.	30.93	N.D.	30.35
$\Delta E^{G}68$	7	N.D.	35.94	N.D.	29.08	N.D.	32.09	N.D.	29.66		N.D.	29.46	N.D.	29.07	N.D.	31.58
contact	8	N.D.	35.5	N.D.	33.83	N.D.	31.79	N.D.	30.32		N.D.	29.77	N.D.	32.02	N.D.	29.79
$\Delta E^{G}68$	9	N.D.	N.D.	N.D.	33.16	N.D.	32.74	N.D.	33.33		N.D.	31.77	N.D.	31.37	N.D.	31.11
contact	10	N.D.	34.55	N.D.	31.23	N.D.	28.44	N.D.	31.07		N.D.	32.99	N.D.	32.42	N.D.	29.15
$\Delta E^{G}68$	11	N.D.	37.15	N.D.	31.65	N.D.	29.18	N.D.	30.31		38.06	30.87	N.D.	31.26	N.D.	27.90
contact	12	N.D.	35.64	N.D.	33.44	39.27	33.84	N.D.	28.53		N.D.	34.12	N.D.	32.69	N.D.	31.35
$\Delta E^{G}68$	13	N.D.	34.66	N.D.	30.73	N.D.	31.06	N.D.	31.93		N.D.	31.38	N.D.	33.76	N.D.	29.01
contact	14	N.D.	35.24	N.D.	32.79	N.D.	30.53	N.D.	28.79		N.D.	28.32	N.D.	30.01	N.D.	27.91
$\Delta E^{G}68$	15	N.D.	38.35	N.D.	32.24	N.D.	31.45	N.D.	30.68		N.D.	31.74	N.D.	29.47	N.D.	29.59
contact	16	N.D.	37.58	N.D.	32.38	N.D.	29.06	N.D.	29.04		N.D.	32.17	N.D.	31.15	N.D.	28.61
$\Delta E^{G}68$	17	N.D.	39.58	N.D.	28.61	N.D.	30.15	39.2	30.79		N.D.	30.97	N.D.	31.31	N.D.	32.10
contact	18	N.D.	N.D.	N.D.	32.2	N.D.	28.76	N.D.	30.62		N.D.	31.95	N.D.	30.44	N.D.	29.61
negative control	1	N.D.	N.D.	N.D.	N.D.	N.D.	N.D.	N.D.	36.48							
	2	N.D.	38.62	N.D.	N.D.	N.D.	36.93	N.D.	39.43							
Muc-1 (B.1) 10^{-1}	1	19.79	35.16													
	2	19.69	34.51													
Muc-1 (B.1) 10^{-2}	1	22.87	36.36													
	2	22.95	N.D.													
Muc-1 (B.1) 10^{-3}	1	26.13	38.07													
	2	26.22	N.D.													
Muc-1 (B.1) 10^{-4}	1	30.03	N.D.													
	2	29.96	N.D.													

Extended Data Table 3. Lung pathology score sheet (addition to Fig. 4, Extended Data Fig. 4)

Raw data of lung pathology analysis, including affected area of atelectasis (Fig. 4c,e), viral antigen detection score (Virus antigen score: 0 = no antigen; 1 = focal; 2 = multifocal; 3 = coalescing; 4 = diffuse) (Fig. 4d,f) and detailed analysis of minor phenotypes in the lung (related to Extended Data Fig. 4e-h).

Abbreviations: G = granulocyte, L = lymphocyte, M = macrophage, P = plasma cell; AEC = alveolar epithelial cell; DAD = diffuse alveolar damage.

Animal ID	1	2	3	4	5	6	10	14	18	1	2	5	6	9	4	8	11	12	13	14	15
Group	ΔE^G68						ΔE^G68 contact			ΔE^G					ΔE^G contact			sham			
Atelectasis %	0	0	0	0	0	0	0	0	0	0	0	0	0	0	19	6	4	33	48	7	65
Virus antigen score	0	0	0	0	0	0	0	0	0	0	0	0	0	0	0	0	0	3	3	3	4
Lung histopathology details: (1 = present in up to 3 foci; 3 = >3 foci)																					
Infiltrates alveolar	0	0	0	0	0	0	0	0	0	1	0	0	1	1	3	1	3	3	3	3	3
predominant cell type: G, L, M, P	/	/	/	/	/	/	/	/	/	M	/	/	M, G	M	M	M	M	M, L	M, L, G	M, L, G	M, L, G
Infiltrates interstitial	0	1	0	0	0	0	0	0	0	1	0	1	1	1	3	1	1	3	3	3	3
predominant cell type: G, L, M, P	/	L, M	/	/	/	/	/	/	/	M, L	/	L, M	M, L, G	L, M	L, M	L, M	M	M, L, G	M, L, G	M, L, G	M, L, G
Infiltrates peribronchial (Incl. glands)	0	0	0	0	0	0	0	0	0	0	0	0	0	1	3	3	3	3	3	3	3
predominant cell type: G, L, M, P	/	/	/	/	/	/	/	/	/	/	/	/	/	M, L	M, L	L, M	M, L	M, L	M, L	M, L	M, L
Necrotizing bronchitis	0	0	0	0	0	0	0	0	0	0	0	0	0	0	1	0	0	1	1	3	1
predominant cell type: G, L, M, P	/	/	/	/	/	/	/	/	/	/	/	/	/	/	M, L	/	/	M, G	M	M, G	M
Infiltrates perivascular	1	1	1	1	0	1	0	0	0	1	0	1	1	3	3	3	3	3	3	3	3
predominant cell type: G, L, M, P	L, M	L, M	L, M	L	/	/	/	/	/	L, M	/	L, M	L, M	M, L	M, L	M, L	M, L	M, L, G	M, L, G	M, L, G	M, L, G
Vasculitis	0	0	0	0	0	0	0	0	0	0	0	0	0	0	0	0	0	3	3	3	3
Immune cell aggregation, vascular activation	0	0	0	0	0	0	0	0	0	0	0	0	0	0	1	1	0	3	3	3	3
Edema alveolar	1	1	1	1	1	1	1	0	0	1	1	1	0	1	1	1	1	3	3	3	3
Necrosis AEC	0	0	0	0	0	0	0	0	0	0	0	0	0	0	3	3	3	3	3	3	3
Diffuse alveolar damage	0	0	0	0	0	0	0	0	0	0	0	0	0	0	0	0	0	0	0	0	0
Hypertrophy/hyperplasia, bronchi	0	0	0	0	0	0	0	0	0	1	0	0	0	0	3	3	3	3	3	3	3
Hyperplasia /hypertrophy type II pneumocytes	0	0	1	0	0	0	0	0	0	1	0	1	0	1	3	3	3	3	3	3	3

Extended Data Table 4. Neutralization data (addition to Fig. 3 and 4)

Serum neutralization data for ΔE^G68 and ΔE^G vaccinated animals, contacts, and sham-treated animals after vaccination and challenge infection against Wuhan (B.1). Note: all values represented with "<dilution" are negative for the indicated dilution or higher dilutions but are not tested for lower dilutions. Values represent the mean from 3 technical replicates, calculated with the Kerber formula (see Methods).

	ID	dpim 19	dpim 33	dpc 5	dpc 14
ΔE^G68	1	<1:32	1:203.2	1:128	
ΔE^G68	2	<1:32	1:322.5	1:161.3	
ΔE^G68	3	<1:64	1:406.4	1:128	
ΔE^G68	4	<1:32	<1:32	1:512	
ΔE^G68	5	<1:32	1:645.1	1:322.5	
ΔE^G68	6	<1:32	1:101.6	1:128	
ΔE^G68	7	<1:32	1:80.6		1:161.3
contact	8				
ΔE^G68	9	<1:32	1:161.3		1:64
contact	10				
ΔE^G68	11	<1:32	1:256		1:101.6
contact	12				
ΔE^G68	13	<1:32	1:161.3		1:128
contact	14	<1:32	1:40.32		<1:32
ΔE^G68	15	<1:32	<1:32		1:256
contact	16				
ΔE^G68	17	<1:32	1:406.4		1:128
contact	18				
ΔE^G	1	<1:128	<1:128	1:512	
ΔE^G	2	<1:128	N.A.	1:256	
ΔE^G	3	<1:128	<1:128		1:322,5
contact	4				1:40,32
ΔE^G	5	<1:512	<1:256	1:101,6	
ΔE^G	6	<1:128	<1:32	1:128	
ΔE^G	7	<1:512	<1:256		1:50,8
contact	8				1:32
ΔE^G	9	<1:256	<1:256	1:1024	
ΔE^G	10	<1:512	<1:256		1:512
contact	11				1:40,32
sham	12			<1:16	
sham	13			1:20,16	
sham	14			<1:16	
sham	15			<1:16	

Supplementary Files

This is a list of supplementary files associated with this preprint. Click to download.

- SupplementaryInformation1.pdf